Optimum Aerodynamic Design via Boundary Control

Antony Jameson

Optimum Aerodynamic Design
via Boundary Control*

Antony Jameson
Department of Mechanical and Aerospace Engineering
Princeton University
Princeton, New Jersey, 08544 U.S.A.

ABSTRACT

These lectures describe the implementation of optimization techniques based on control theory for airfoil and wing design. In previous studies [10, 11] it was shown that control theory could be used to devise an effective optimization procedure for two-dimensional profiles in which the shape is determined by a conformal transformation from a unit circle, and the control is the mapping function. Recently the method has been implemented in an alternative formulation which does not depend on conformal mapping, so that it can more easily be extended to treat general configurations [16]. The method has also been extended to treat the Euler equations, and results are presented for both two and three dimensional cases, including the optimization of a swept wing.

1 FORMULATION OF THE DESIGN PROBLEM AS A CONTROL PROBLEM

Ultimately, the designer seeks to optimize the geometric shape of a configuration taking into account the trade-offs between aerodynamic performance, structure weight, and the requirement for internal volume to contain fuel and payload. The subtlety and complexity of fluid flow is such that it is unlikely that repeated trials in an interactive analysis and design procedure can lead to a truly optimum design. Progress toward automatic design has been restricted by the extreme computing costs that might be incurred from brute force numerical optimization. However, useful design methods have been devised for various simplified cases, such as two-dimensional airfoils in viscous flows [17] and wings in inviscid flows. The computational costs for these methods result directly from the vast number of flow solutions that are required to obtain a converged design.

Alternatively, it has been recognized that the designer generally has an idea of the kind of pressure distribution that will lead to the desired performance. Thus, it is useful to consider the inverse problem of calculating the shape that will lead to a given pressure distribution. The

method is advantageous, since only one flow solution is required to obtain the desired design. Unfortunately, a physically realizable shape may not necessarily exist, unless the pressure distribution satisfies certain constraints. Thus the problem must be very carefully formulated.

The problem of designing a two-dimensional profile to attain a desired pressure distribution was first studied by Lighthill, who solved it for the case of incompressible flow with a conformal mapping of the profile to a unit circle [13]. The speed over the profile is

$$q = \frac{1}{h} |\nabla \phi|,$$

where ϕ is the potential which is known for incompressible flow and h is the modulus of the mapping function. The surface value of h can be obtained by setting $q = q_d$, where q_d is the desired speed, and since the mapping function is analytic, it is uniquely determined by the value of h on the boundary. A solution exists for a given speed q_∞ at infinity only if

$$\frac{1}{2\pi} \oint q \, d\theta = q_\infty,$$

and there are additional constraints on q if the profile is required to be closed.

The difficulty that the objective may be unattainable can be circumvented by regarding the design problem as a control problem in which the control is the shape of the boundary. A variety of alternative formulations of the design problem can then be treated systematically within the framework of the mathematical theory for control of systems governed by partial differential equations [14]. This approach to optimal aerodynamic design was introduced by Jameson [10, 11], who examined the design problem for compressible flow with shock waves, and devised adjoint equations to determine the gradient for both potential flow and also flows governed by the Euler equations. More recently Ta'asan, Kuruvila, and Salas, implemented a one shot approach in which the constraint represented by the flow equations is only required to be satisfied by the final converged solution [20]. Pironneau has also studied the use of control theory for optimum shape design of systems governed by elliptic equations [15].

Suppose that the control is defined by a function $\mathcal{F}(\xi)$ of some independent variable ξ or in the discrete case a vector with components $\mathcal{F}_i$. Also suppose that the desired objective is measured by a cost function I. This may, for example, measure the deviation from a desired surface pressure distribution, but it can also represent other measures of performance such as lift and drag. Thus the design problem is recast into a numerical optimization procedure. This has the advantage that if the objective, say, of a target pressure distribution, is unattainable, it is still possible to find a minimum of the cost function. Now a variation $\delta\mathcal{F}$ in the control produces a variation δI in the cost. Following control theory, δI can be expressed to first order as an inner product

$$\delta I = (\mathcal{G}, \delta\mathcal{F}),$$

where the gradient $\mathcal{G}$ is independent of the particular variation $\delta\mathcal{F}$, and can be determined by solving an adjoint equation. For a discrete system of equations

$$(\mathcal{G}, \delta\mathcal{F}) \equiv \sum \mathcal{G}_i \delta\mathcal{F}_i$$

and for an infinitely dimensional system

$$(\mathcal{G}, \delta\mathcal{F}) \equiv \int \mathcal{G}(\xi)\delta\mathcal{F}\,d\xi.$$

In either case, if one makes a shape change

$$\delta\mathcal{F} = -\lambda\mathcal{G}, \qquad (1)$$

where λ is sufficiently small and positive, then

$$\delta I = -\lambda(\mathcal{G}, \mathcal{G}) < 0$$

assuring a reduction in I.

For flow about an airfoil or wing, the aerodynamic properties which define the cost function are functions of the flow-field variables (w) and the physical location of the boundary, which may be represented by the function $\mathcal{F}$, say. Then

$$I = I(w, \mathcal{F}),$$

and a change in $\mathcal{F}$ results in a change

$$\delta I = \frac{\partial I^T}{\partial w}\delta w + \frac{\partial I^T}{\partial \mathcal{F}}\delta\mathcal{F}, \qquad (2)$$

in the cost function. As pointed out by Baysal and Eleshaky [2] each term in (2), except for δw, can be easily obtained. $\frac{\partial I}{\partial w}$ and $\frac{\partial I}{\partial \mathcal{F}}$ can be obtained directly without a flowfield evaluation since they are partial derivatives. $\delta\mathcal{F}$ can be determined by either working out the exact analytical values from a mapping, or by successive grid generation for each design variable, so long as this cost is significantly less then the cost of the flow solution. Brute force methods evaluate the gradient by making a small change in each design variable separately, and then recalculate both the grid and flow-field variables. This

requires a number of additional flow calculations equal to the number of design variables. Using control theory, the governing equations of the flowfield are introduced as a constraint in such a way that the final expression for the gradient does not require reevaluation of the flowfield. In order to achieve this δw must be eliminated from (2). The governing equation R expresses the dependence of w and $\mathcal{F}$ within the flowfield domain D,

$$R(w, \mathcal{F}) = 0,$$

Thus δw is determined from the equation

$$\delta R = \left[\frac{\partial R}{\partial w}\right]\delta w + \left[\frac{\partial R}{\partial \mathcal{F}}\right]\delta\mathcal{F} = 0. \qquad (3)$$

Next, introducing a Lagrange Multiplier ψ, we have

$$
\begin{aligned}
\delta I &= \frac{\partial I^T}{\partial w}\delta w + \frac{\partial I^T}{\partial \mathcal{F}}\delta\mathcal{F} - \psi^T\left(\left[\frac{\partial R}{\partial w}\right]\delta w + \left[\frac{\partial R}{\partial \mathcal{F}}\right]\delta\mathcal{F}\right) \\
&= \left\{\frac{\partial I^T}{\partial w} - \psi^T\left[\frac{\partial R}{\partial w}\right]\right\}\delta w + \left\{\frac{\partial I^T}{\partial \mathcal{F}} - \psi^T\left[\frac{\partial R}{\partial \mathcal{F}}\right]\right\}\delta\mathcal{F}
\end{aligned}
$$

Choosing ψ to satisfy the adjoint equation

$$\left[\frac{\partial R}{\partial w}\right]^T \psi = \frac{\partial I}{\partial w} \qquad (4)$$

the first term is eliminated, and we find that

$$\delta I = \mathcal{G}\delta\mathcal{F} \qquad (5)$$

where

$$\mathcal{G} = \frac{\partial I^T}{\partial \mathcal{F}} - \psi^T\left[\frac{\partial R}{\partial \mathcal{F}}\right].$$

The advantage is that (5) is independent of δw, with the result that the gradient of I with respect to an arbitrary number of design variables can be determined without the need for additional flow-field evaluations. The main cost is in solving the adjoint equation (4). In general, the adjoint problem is about as complex as a flow solution. If the number of design variables is large, the cost differential between one adjoint solution and the large number of flowfield evaluations required to determine the gradient by brute force becomes compelling. Instead of introducing a Lagrange multiplier, ψ, one can solve (3) for δw as

$$\delta w = -\left[\frac{\partial R}{\partial w}\right]^{-1}\left[\frac{\partial R}{\partial \mathcal{F}}\right]\delta\mathcal{F},$$

and insert the result in (2). This is the implicit gradient approach, which is essentially equivalent to the control theory approach, as has been pointed out by Shubin and Frank [18, 19]. In any event there is an advantage in determining the gradient $\mathcal{G}$ by the solution of the adjoint equation.

After making such a modification, the gradient can be recalculated and the process repeated to follow a path of steepest descent (1) until a minimum is reached. In order

to avoid violating constraints, such as a minimum acceptable wing thickness, the gradient may be projected into the allowable subspace within which the constraints are satisfied. In this way one can devise procedures which must necessarily converge at least to a local minimum, and which can be accelerated by the use of more sophisticated descent methods such as conjugate gradient or quasi-Newton algorithms. There is the possibility of more than one local minimum, but in any case the method will lead to an improvement over the original design. Furthermore, unlike the traditional inverse algorithms, any measure of performance can be used as the cost function.

The next section presents the formulation for the case of airfoils in transonic flow. The governing equation is taken to be the transonic potential flow equation, and the profile is generated by conformal mapping from a unit circle. Thus the control is taken to be the modulus of the mapping function on the boundary. This leads to a generalization of Lighthill's method both to compressible flow, and to design for more general criteria. Numerical results are presented in Section 3. The mathematical development resembles, in certain respects, the method of calculating transonic potential flow developed by Bristeau, Pironneau, Glowinski, Periaux, Perrier and Poirier, who reformulated the solution of the flow equations as a least squares problem in control theory [3].

2 AIRFOIL DESIGN FOR POTENTIAL FLOW USING CONFORMAL MAPPING

Consider the case of two-dimensional compressible inviscid flow. In the absence of shock waves, an initially irrotational flow will remain irrotational, and we can assume that the velocity vector q is the gradient of a potential ϕ. In the presence of weak shock waves this remains a fairly good approximation.

1a: z-Plane.   1b: σ-Plane.
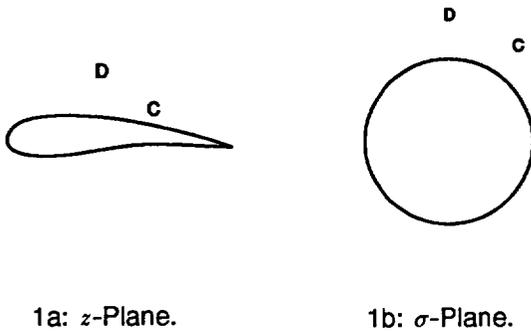
Figure 1: Conformal Mapping.

Let p, ρ, c, and M be the pressure, density, speed-of-sound, and Mach number q/c. Then the potential flow equation is

$$\nabla \cdot (\rho \nabla \phi) = 0, \qquad (6)$$

where the density is given by

$$\rho = \left\{ 1 + \frac{\gamma - 1}{2} M_\infty^2 \left(1 - q^2 \right) \right\}^{\frac{1}{(\gamma - 1)}}, \qquad (7)$$

while

$$p = \frac{\rho^\gamma}{\gamma M_\infty^2}, \quad c^2 = \frac{\gamma p}{\rho}. \qquad (8)$$

Here M_∞ is the Mach number in the free stream, and the units have been chosen so that p and q have a value of unity in the far field.

Suppose that the domain D exterior to the profile C in the z-plane is conformally mapped on to the domain exterior to a unit circle in the σ-plane as sketched in Figure 1. Let R and θ be polar coordinates in the σ-plane, and let r be the inverted radial coordinate $\frac{1}{R}$. Also let h be the modulus of the derivative of the mapping function

$$h = \left| \frac{dz}{d\sigma} \right|. \qquad (9)$$

Now the potential flow equation becomes

$$\frac{\partial}{\partial \theta} (\rho \phi_\theta) + r \frac{\partial}{\partial r} (r \rho \phi_r) = 0 \quad \text{in } D, \qquad (10)$$

where the density is given by equation (7), and the circumferential and radial velocity components are

$$u = \frac{r \phi_\theta}{h}, \quad v = \frac{r^2 \phi_r}{h}, \qquad (11)$$

while

$$q^2 = u^2 + v^2. \qquad (12)$$

The condition of flow tangency leads to the Neumann boundary condition

$$v = \frac{1}{h} \frac{\partial \phi}{\partial r} = 0 \quad \text{on } C. \qquad (13)$$

In the far field, the potential is given by an asymptotic estimate, leading to a Dirichlet boundary condition at $r = 0$ [6].

Suppose that it is desired to achieve a specified velocity distribution q_d on C. Introduce the cost function

$$I = \frac{1}{2} \int_C (q - q_d)^2 \, d\theta,$$

The design problem is now treated as a control problem where the control function is the mapping modulus h, which is to be chosen to minimize I subject to the constraints defined by the flow equations (6–13).

A modification δh to the mapping modulus will result in variations $\delta \phi$, δu, δv, and $\delta \rho$ to the potential, velocity components, and density. The resulting variation in the cost will be

$$\delta I = \int_C (q - q_d) \, \delta q \, d\theta, \qquad (14)$$

3

where, on C, $q = u$. Also,

$$\delta u = r\frac{\delta\phi_\theta}{h} - u\frac{\delta h}{h}, \quad \delta v = r^2\frac{\delta\phi_r}{h} - v\frac{\delta h}{h},$$

while according to equation (7)

$$\frac{\partial\rho}{\partial u} = -\frac{\rho u}{c^2}, \quad \frac{\partial\rho}{\partial v} = -\frac{\rho v}{c^2}.$$

It follows that $\delta\phi$ satisfies

$$L\delta\phi = -\frac{\partial}{\partial\theta}\left(\rho M^2\phi_\theta\frac{\delta h}{h}\right) - r\frac{\partial}{\partial r}\left(\rho M^2 r\phi_r\frac{\delta h}{h}\right)$$

where

$$L \equiv \frac{\partial}{\partial\theta}\left\{\rho\left(1 - \frac{u^2}{c^2}\right)\frac{\partial}{\partial\theta} - \frac{\rho uv}{c^2}r\frac{\partial}{\partial r}\right\}$$
$$+ r\frac{\partial}{\partial r}\left\{\rho\left(1 - \frac{v^2}{c^2}\right)r\frac{\partial}{\partial r} - \frac{\rho uv}{c^2}\frac{\partial}{\partial\theta}\right\}. \quad (15)$$

Then, if ψ is any periodic differentiable function which vanishes in the far field,

$$\int_D \frac{\psi}{r^2}L\,\delta\phi\,dS = \int_D \rho M^2\nabla\phi\cdot\nabla\psi\frac{\delta h}{h}\,dS, \quad (16)$$

where dS is the area element $r\,dr\,d\theta$, and the right hand side has been integrated by parts.

Now we can augment equation (14) by subtracting the constraint (16). The auxiliary function ψ then plays the role of a Lagrange multiplier. Thus,

$$\delta I = \int_C (q - q_d)q\frac{\delta h}{h}\,d\theta - \int_C \delta\phi\frac{\partial}{\partial\theta}\left(\frac{q - q_d}{h}\right)\,d\theta$$
$$- \int_D \frac{\psi}{r^2}L\delta\psi\,dS + \int_D \rho M^2\nabla\phi\cdot\nabla\psi\frac{\delta h}{h}\,dS.$$

Now suppose that ψ satisfies the adjoint equation

$$L\psi = 0 \quad \text{in } D \quad (17)$$

with the boundary condition

$$\frac{\partial\psi}{\partial r} = \frac{1}{\rho}\frac{\partial}{\partial\theta}\left(\frac{q - q_d}{h}\right) \quad \text{on } C. \quad (18)$$

Then, integrating by parts,

$$\int_D \frac{\psi}{r^2}L\delta\phi\,dS = -\int_C \rho\psi_r\delta\phi\,d\theta,$$

and

$$\delta I = -\int_C (q - q_d)q\frac{\delta h}{h}\,d\theta$$
$$+ \int_D \rho M^2\nabla\phi\cdot\nabla\psi\frac{\delta h}{h}\,dS. \quad (19)$$

Here the first term represents the direct effect of the change in the metric, while the area integral represents a correction for the effect of compressibility. When the second term is deleted the method reduces to a variation of Lighthill's method [13].

Equation (19) can be further simplified to represent δI purely as a boundary integral because the mapping function is fully determined by the value of its modulus on the boundary. Set

$$\log\frac{dz}{d\sigma} = \mathcal{F} + i\beta,$$

where

$$\mathcal{F} = \log\left|\frac{dz}{d\sigma}\right| = \log h,$$

and

$$\delta\mathcal{F} = \frac{\delta h}{h}.$$

Then $\mathcal{F}$ satisfies Laplace's equation

$$\Delta\mathcal{F} = 0 \quad \text{in } D,$$

and if there is no stretching in the far field, $\mathcal{F} \to 0$. Also $\delta\mathcal{F}$ satisfies the same conditions. Introduce another auxiliary function P which satisfies

$$\Delta P = \rho M^2\nabla\psi\cdot\nabla\psi \quad \text{in } D, \quad (20)$$

and

$$P = 0 \quad \text{on } C.$$

Then, the area integral in equation (19) is

$$\int_D \Delta P\,\delta\mathcal{F}\,dS = \int_C \delta\mathcal{F}\frac{\partial P}{\partial r}\,d\theta - \int_D P\Delta\,\delta\mathcal{F}\,dS,$$

and finally

$$\delta I = \int_C \mathcal{G}\,\delta\mathcal{F}\,d\theta,$$

where $\mathcal{F}_c$ is the boundary value of $\mathcal{F}$, and

$$\mathcal{G} = \frac{\partial P}{\partial r} - (q - q_d)q. \quad (21)$$

This suggests setting

$$\delta\mathcal{F}_c = -\lambda\mathcal{G}$$

so that if λ is a sufficiently small positive quantity

$$\delta I = -\int_C \lambda\mathcal{G}^2\,d\theta < 0.$$

Arbitrary variations in $\mathcal{F}$ cannot, however, be admitted. The condition that $\mathcal{F} \to 0$ in the far field, and also the requirement that the profile should be closed, imply constraints which must be satisfied by $\mathcal{F}$ on the boundary C. Suppose that $\log\left(\frac{dz}{d\sigma}\right)$ is expanded as a power series

$$\log\left(\frac{dz}{d\sigma}\right) = \sum_{n=o}^\infty \frac{c_n}{\sigma^n}, \quad (22)$$

4

where only negative powers are retained, because otherwise $\left(\frac{dz}{d\sigma}\right)$ would become unbounded for large σ. The condition that $\mathcal{F} \to 0$ as $\sigma \to \infty$ implies

$$c_o = 0.$$

Also, the change in z on integration around a circuit is

$$\Delta z = \int \frac{dz}{d\sigma} \, d\sigma = 2\pi i \, c_1,$$

so the profile will be closed only if

$$c_1 = 0.$$

In order to satisfy these constraints, we can project $\mathcal{G}$ onto the admissible subspace for $\mathcal{F}_c$ by setting

$$c_o = c_1 = 0. \qquad (23)$$

Then the projected gradient $\bar{\mathcal{G}}$ is orthogonal to $\mathcal{G} - \bar{\mathcal{G}}$, and if we take

$$\delta \mathcal{F}_c = -\lambda \bar{\mathcal{G}},$$

it follows that to first order

$$
\begin{aligned}
\delta I &= -\int_C \lambda \mathcal{G} \bar{\mathcal{G}} \, d\theta = -\int_C \lambda \left(\bar{\mathcal{G}} + \mathcal{G} - \bar{\mathcal{G}} \right) \mathcal{G} \, d\theta \\
&= -\int_C \lambda \bar{\mathcal{G}}^2 \, d\theta < 0.
\end{aligned}
$$

If the flow is subsonic, this procedure should converge toward the desired speed distribution since the solution will remain smooth, and no unbounded derivatives will appear. If, however, the flow is transonic, one must allow for the appearance of shock waves in the trial solutions, even if q_d is smooth. Then $q - q_d$ is not differentiable. This difficulty can be circumvented by a more sophisticated choice of the cost function. Consider the choice

$$I = \frac{1}{2} \int_C \left(\lambda_1 \mathcal{Z}^2 + \lambda_2 \left(\frac{d\mathcal{Z}}{d\theta} \right)^2 \right) d\theta, \qquad (24)$$

where λ_1 and λ_2 are parameters, and the periodic function $\mathcal{Z}(\theta)$ satisfies the equation

$$\lambda_1 \mathcal{Z} - \lambda_2 \frac{d^2 \mathcal{Z}}{d\theta^2} = q - q_d. \qquad (25)$$

Then,

$$
\begin{aligned}
\delta I &= \int_C \left(\lambda_1 \mathcal{Z} \, \delta \mathcal{Z} + \lambda_2 \frac{d\mathcal{Z}}{d\theta} \frac{d}{d\theta} \delta \mathcal{Z} \right) d\theta \\
&= \int_C \mathcal{Z} \left(\lambda_1 \delta \mathcal{Z} - \lambda_2 \frac{d^2}{d\theta^2} \delta \mathcal{Z} \right) d\theta = \int_C \mathcal{Z} \, \delta q \, d\theta.
\end{aligned}
$$

Thus, $\mathcal{Z}$ replaces $q - q_d$ in the previous formulas, and if one modifies the boundary condition (18) to

$$\frac{\partial \psi}{\partial r} = \frac{1}{\rho} \frac{\partial}{\partial \theta} \left(\frac{\mathcal{Z}}{h} \right) \quad \text{on } C, \qquad (26)$$

the formula for the gradient becomes

$$\mathcal{G} = \frac{\partial P}{\partial r} - \mathcal{Z} q \qquad (27)$$

instead of equation (21). Smoothing can also be introduced directly in the descent procedure by choosing $\delta \mathcal{F}_c$ to satisfy

$$\delta \mathcal{F}_c - \frac{\partial}{\partial \theta} \beta \frac{\partial}{\partial \theta} \delta \mathcal{F}_c = -\lambda \mathcal{G}, \qquad (28)$$

where β is a smoothing parameter. Then to first order

$$
\begin{aligned}
\int \mathcal{G} \, \delta \mathcal{F} &= -\frac{1}{\lambda} \int \left(\delta \mathcal{F}_c^2 - \delta \mathcal{F}_c \frac{\partial}{\partial \theta} \beta \frac{\partial}{\partial \theta} \delta \mathcal{F}_c \right) d\theta \\
&= -\frac{1}{\lambda} \int \left(\delta \mathcal{F}_c^2 + \beta \left(\frac{\partial}{\partial \theta} \delta \mathcal{F}_c \right)^2 \right) d\theta < 0.
\end{aligned}
$$

The smoothed correction should now be projected onto the admissable subspace.

The final design procedure is thus as follows. Choose an initial profile and corresponding mapping function $\mathcal{F}$. Then:

1. Solve the flow equations (6–13) for ϕ, u, v, q, ρ.

2. Solve the ordinary differential equation (25) for $\mathcal{Z}$.

3. Solve the adjoint equation (15 and 17) or ψ subject to the boundary condition (26).

4. Solve the auxiliary Poisson equation (20) for P.

5. Evaluate $\mathcal{G}$ by equation (27)

6. Correct the boundary mapping function $\mathcal{F}_c$ by $\delta \mathcal{F}_c$ calculated from equation (28), projected onto the admissable subspace defined by (23).

7. Return to step 1.

3   NUMERICAL TESTS OF OPTIMAL AIRFOIL DESIGN FOR POTENTIAL FLOW USING CONFORMAL MAPPING

The practical realization of the design procedure depends on the availability of sufficiently fast and accurate numerical procedures for the implementation of the essential steps, in particular the solution of both the flow and the adjoint equations. If the numerical procedures are not accurate enough, the resulting errors in the gradient may impair or prevent the convergence of the descent procedure. If the procedures are too slow, the cumulative computing time may become excessive. In this case, it was possible to build the design procedure around the author's computer program FLO36, which solves the transonic potential flow equation in conservation form in a domain mapped to the unit disk. The solution is obtained by a very rapid multigrid alternating direction method. The original

5

scheme is described in Reference [7]. The program has been much improved since it was originally developed, and well converged solutions of transonic flows on a mesh with 128 cells in the circumferential direction and 32 cells in the radial direction are typically obtained in 5-20 multigrid cycles. The scheme uses artificial dissipative terms to introduce upwind biasing which simulates the rotated difference scheme [6], while preserving the conservation form. The alternating direction method is a generalization of conventional alternating direction methods, in which the scalar parameters are replaced by upwind difference operators to produce a scheme which remains stable when the type changes from elliptic to hyperbolic as the flow becomes locally supersonic [7]. The conformal mapping is generated by a power series of the form of equation (22) with an additional term

$$\left(1 - \frac{\epsilon}{\phi}\right) \log\left(1 - \frac{1}{\sigma}\right)$$

to allow for a wedge angle ϵ at the trailing edge. The coefficients are determined by an iterative process with the aid of fast Fourier transforms [6].

The adjoint equation has a form very similar to the flow equation. While it is linear in its dependent variable, it also changes type from elliptic in subsonic zones of the flow to hyperbolic in supersonic zones of the flow. Thus, it was possible to adapt exactly the same algorithm to solve both the adjoint and the flow equations, but with reverse biasing of the difference operators in the downwind direction in the adjoint equation, corresponding to the reversed direction of the zone of dependence. The Poisson equation (20) is solved by the Buneman algorithm.

An alternative procedure would be to derive the exact adjoint equation corresponding to the discrete equations which approximate the potential flow equation. This would produce the exact derivative of the discrete cost function with respect to the discrete control, at the expense of very complicated formulas and a costly inversion procedure. The discrete adjoint equation would then be a particular discretization of the differential adjoint equation corresponding precisely to the discretization used for the flow equation. The efficiency of the present approach, which uses separate discretizations of the flow and adjoint equations, depends on the fact that in the limit of zero mesh width the discrete adjoint solution converges to the true adjoint solution. This allows the use of a rather simple discretization of the adjoint equation modeled after the discretization of the flow equation. Numerical experiments confirm that in practice separate discretizations of the flow and adjoint equations yields good convergence to an optimum solution.

As an example of the application of the method, Figure 3 presents a calculation in which an airfoil was redesigned to improve its transonic performance by reducing the pressure drag induced by the appearance of a shock wave. The drag coefficient was therefore included in the cost function so that equation (24) is replaced by

$$I = \frac{1}{2} \int_C \left(\lambda_1 \mathcal{Z}^2 + \lambda_2 \left(\frac{d\mathcal{Z}}{d\theta}\right)^2\right) d\theta + \lambda_3 C_d,$$

where λ_3 is a parameter which may be varied to alter the trade-off between drag reduction and deviation from the desired pressure distribution. Representing the drag as

$$D = \int_C (p - p_\infty) \frac{dy}{d\theta} d\theta,$$

the procedure of Section 2 may be used to determine the gradient by solving the adjoint equation with a modified boundary condition. A penalty on the desired pressure distribution is still needed to avoid a situation in which the optimum shape is a flat plate with no lift and no drag.

It was also desired to preserve the subsonic characteristics of the airfoil. Therefore two design points were specified, Mach 0.20 and Mach 0.720, and in each case the lift coefficient was forced to be 0.6. The composite cost function was taken to be the sum of the values of the cost function at the two design points. The transonic drag coefficient was reduced from 0.0191 to 0.0001 in 8 design cycles. In order to achieve this reduction the airfoil had to be modified so that its subsonic pressure distribution became more peaky at the leading edge. This is consistent with the results of experimental research on transonic airfoils, in which it has generally been found necessary to have a peaky subsonic presure distribution in order to delay the onset of the transonic drag rise. It is also important to control the adverse pressure gradient on the rear upper surface, which can lead to premature separation of the viscous boundary layer. It can be seen that there is no steepening of this gradient due to the redesign.

4 DESIGN FOR POTENTIAL FLOW USING A FINITE VOLUME DISCRETIZATION SCHEME

While the use of conformal mapping, as it has been presented in sections 2 and 3, leads to an effective design method for two dimensional profiles, it is not easy to treat more complex configurations because of the difficulty in devising appropriate numerical mapping methods. Moreover, conformal mapping is limited to two dimensional transformations. In this section an alternative formulation using a general coordinate transformation is adopted. This is intended to be a precursor to the three dimensional problem.

Consider the case of two-dimensional compressible inviscid flow. A general transformation from cartesian coordinates x and y to the coordinates ξ and η can be represented by the transformation

$$K = \begin{bmatrix} \frac{\partial x}{\partial \xi} & \frac{\partial x}{\partial \eta} \\ \frac{\partial y}{\partial \xi} & \frac{\partial y}{\partial \eta} \end{bmatrix}.$$

The potential flow equation can be written in divergence form as

$$\frac{\partial}{\partial x}(\rho u) + \frac{\partial}{\partial y}(\rho v) = 0 \quad \text{in } D, \qquad (29)$$

where u and v represent the Cartesian velocity components. The coordinate transformations may be defined

$$\left\{ \begin{array}{c} u \\ v \end{array} \right\} = \left\{ \begin{array}{c} \phi_x \\ \phi_y \end{array} \right\} = \left[\begin{array}{cc} \frac{\partial \xi}{\partial x} & \frac{\partial \eta}{\partial x} \\ \frac{\partial \xi}{\partial y} & \frac{\partial \eta}{\partial y} \end{array} \right] \left\{ \begin{array}{c} \phi_\xi \\ \phi_\eta \end{array} \right\}$$

$$= K^{T^{-1}} \left\{ \begin{array}{c} \phi_\xi \\ \phi_\eta \end{array} \right\}. \qquad (30)$$

Also

$$\left\{ \begin{array}{c} \phi_\xi \\ \phi_\eta \end{array} \right\} = \left[\begin{array}{cc} \frac{\partial x}{\partial \xi} & \frac{\partial y}{\partial \xi} \\ \frac{\partial x}{\partial \eta} & \frac{\partial y}{\partial \eta} \end{array} \right] \left\{ \begin{array}{c} \phi_x \\ \phi_y \end{array} \right\} = K^T \left\{ \begin{array}{c} \phi_x \\ \phi_y \end{array} \right\},$$

Then

$$\frac{\partial}{\partial \xi}(\rho J U) + \frac{\partial}{\partial \eta}(\rho J V) = 0 \quad \text{in } D. \qquad (31)$$

where J is the Jacobian

$$J = \det(K) = \frac{\partial x}{\partial \xi}\frac{\partial y}{\partial \eta} - \frac{\partial x}{\partial \eta}\frac{\partial y}{\partial \xi}.$$

Here, U and V represent the contravariant velocities

$$\left\{ \begin{array}{c} U \\ V \end{array} \right\} = \frac{1}{J} \left[\begin{array}{cc} \frac{\partial y}{\partial \eta} & -\frac{\partial x}{\partial \eta} \\ -\frac{\partial y}{\partial \xi} & \frac{\partial x}{\partial \xi} \end{array} \right] \left\{ \begin{array}{c} u \\ v \end{array} \right\}$$

$$= = K^{-1} \left\{ \begin{array}{c} u \\ v \end{array} \right\} = K^{-1} K^{T^{-1}} \left\{ \begin{array}{c} \phi_\xi \\ \phi_\eta \end{array} \right\}$$

Thus,

$$U = A_{11}\phi_\xi + A_{12}\phi_\eta \qquad (32)$$

$$V = A_{12}\phi_\xi + A_{22}\phi_\eta. \qquad (33)$$

where

$$A = (K^T K)^{-1} = \left[\begin{array}{cc} A_{11} & A_{12} \\ A_{12} & A_{22} \end{array} \right]$$

Consider first the case in which the cost function is defined such as to achieve a target speed distribution:

$$I = \frac{1}{2} \int_C (q - q_d)^2 \, ds$$

$$= \frac{1}{2} \int_C (q - q_d)^2 \left(\frac{ds}{d\xi}\right) d\xi, \qquad (34)$$

where q_d is the desired speed distribution and C is the airfoil surface.

The design problem is now treated as a control problem where the control function is the airfoil shape, which is to be chosen to minimize I subject to the constraints

defined by the flow equations (29–33). The first variation of the cost function is

$$\delta I = \int_C (q - q_d)\delta q \left(\frac{ds}{d\xi}\right) d\xi$$

$$+ \frac{1}{2} \int_C (q - q_d)^2 \, \delta \left(\frac{ds}{d\xi}\right) d\xi$$

$$= \int_C (q - q_d)\frac{\partial (\delta\phi)}{\partial \xi} d\xi$$

$$+ \frac{1}{2} \int_C (q - q_d)^2 \, \delta \left(\frac{ds}{d\xi}\right) d\xi$$

$$+ \int_C (q - q_d)\frac{\partial \phi}{\partial \xi} \delta \left(\frac{d\xi}{ds}\right)\frac{ds}{d\xi} d\xi, \qquad (35)$$

since on the wall

$$q_w = \frac{\partial \phi}{\partial s} = \frac{\partial \phi}{\partial \xi}\frac{\partial \xi}{\partial s}.$$

In general we need to find how a modification to the airfoil geometry causes a variation $\delta\phi$, as well a variation in the grid parameters $\delta A_{11}, \delta A_{12}, \delta A_{22}$, and δJ. The variations in U, V and ρ are

$$\delta U = \delta(A_{11})\phi_\xi + A_{11}\delta\phi_\xi + \delta(A_{12})\phi_\eta + A_{12}\delta\phi_\eta$$

$$\delta V = \delta(A_{12})\phi_\xi + A_{12}\delta\phi_\xi + \delta(A_{22})\phi_\eta + A_{22}\delta\phi_\eta$$

$$\delta\rho = -\frac{\rho}{c^2}\left[U\frac{\partial}{\partial \xi} + V\frac{\partial}{\partial \eta}\right]\delta\phi$$

$$-\frac{\rho}{2c^2}\left[\delta A_{11}\phi_\xi^2 + 2\delta A_{12}\phi_\eta\phi_\xi + \delta A_{22}\phi_\eta^2\right].$$

It follows that $\delta\phi$ satisfies

$$L\delta\phi = -\frac{\partial}{\partial \xi}Q(\delta J, \delta A_{11}, \delta A_{12}, \delta A_{22})$$

$$-\frac{\partial}{\partial \eta}P(\delta J, \delta A_{11}, \delta A_{12}, \delta A_{22}), \qquad (36)$$

where

$$L \equiv \frac{\partial}{\partial \xi}\left[\begin{array}{c} \rho J\left(A_{11} - \frac{U^2}{c^2}\right)\frac{\partial}{\partial \xi} \\ +\rho J\left(A_{12} - \frac{UV}{c^2}\right)\frac{\partial}{\partial \eta} \end{array} \right]$$

$$+ \frac{\partial}{\partial \eta}\left[\begin{array}{c} \rho J\left(A_{12} - \frac{UV}{c^2}\right)\frac{\partial}{\partial \xi} \\ +\rho J\left(A_{22} - \frac{V^2}{c^2}\right)\frac{\partial}{\partial \eta} \end{array} \right] \qquad (37)$$

and

$$Q(\delta J, \delta A_{11}, \delta A_{12}, \delta A_{22}) = \rho U \delta J$$

$$+\rho J\phi_\xi\left(1 - \frac{U\phi_\xi}{2c^2}\right)\delta A_{11}$$

$$+\rho J\phi_\eta\left(1 - \frac{U\phi_\xi}{c^2}\right)\delta A_{12}$$

$$+\rho J\phi_\eta\left(-\frac{U\phi_\eta}{2c^2}\right)\delta A_{22}$$

$$P(\delta J, \delta A_{11}, \delta A_{12}, \delta A_{22}) = \rho V \delta J$$

$$+ \rho J \phi_\eta \left(1 - \frac{V\phi_\eta}{2c^2}\right) \delta A_{22}$$

$$+ \rho J \phi_\xi \left(1 - \frac{V\phi_\eta}{c^2}\right) \delta A_{12}$$

$$+ \rho J \phi_\xi \left(-\frac{V\phi_\xi}{2c^2}\right) \delta A_{11}.$$

If ψ is any periodic function vanishing in the far field, equation (36) can be multiplied by ψ and integrated over the domain. After integrating the right hand side by parts we arrive at

$$\int_D \psi L \delta \phi \, d\xi d\eta = \int_D \frac{\partial \psi}{\partial \xi} Q + \frac{\partial \psi}{\partial \eta} P \, d\xi d\eta$$

$$+ \int_C \left\{ \psi \rho J \left[\delta A_{12} \phi_\xi + \delta A_{22} \phi_\eta \right] \right\} d\xi. \quad (38)$$

Now subtracting (38) from (35),

$$\delta I = - \int_C \frac{\partial (q - q_d)}{\partial \xi} \delta \phi \, d\xi$$

$$+ \int_C \frac{1}{2} (q - q_d)^2 \, \delta \left(\frac{ds}{d\xi}\right) \, d\xi$$

$$+ \int_C (q - q_d) \frac{\partial \phi}{\partial \xi} \delta \left(\frac{d\xi}{ds}\right) \frac{ds}{d\xi} \, d\xi$$

$$- \int_D \psi L \delta \phi \, d\xi d\eta$$

$$+ \int_D \frac{\delta \psi}{\delta \xi} Q + \frac{\delta \psi}{\delta \eta} P \, d\xi d\eta$$

$$+ \int_C \left\{ \psi \rho J \left[\delta A_{12} \phi_\xi + \delta A_{22} \phi_\eta \right] \right\} d\xi.$$

Then setting up the adjoint system we have

$$L\psi = 0 \quad \text{in } D, \quad (39)$$

with the boundary condition

$$\rho J \left(A_{12} \psi_\xi + A_{22} \phi_\eta \right) = -\frac{\partial}{\partial \xi} (q - q_d). \quad (40)$$

After applying the second form of Green's theorem to (39) we get

$$\int_D \psi L \delta \phi \, dS = \int_C \left\{ \psi \rho J \left[\delta A_{12} \phi_\xi + \delta A_{22} \phi_\eta \right] \right\} d\xi$$

$$+ \int_C \left\{ \delta \phi \rho J \left[\delta A_{12} \psi_\xi + \delta A_{22} \psi_\eta \right] \right\} d\xi.$$

Finally the variation can be defined as

$$\delta I = \frac{1}{2} \int_C (q - q_d)^2 \, \delta \left(\frac{ds}{d\xi}\right) \, d\xi$$

$$+ \int_C (q - q_d) \frac{\partial \phi}{\partial \xi} \delta \left(\frac{d\xi}{ds}\right) \frac{ds}{d\xi} \, d\xi$$

$$+ \int_D \frac{\partial \psi}{\partial \xi} Q + \frac{\partial \psi}{\partial \eta} P \, d\xi d\eta. \quad (41)$$

No general analytic grid transformation is generally available for the finite volume formulation. Furthermore, the variation with respect to the grid quantities is now spread into δA_{11}, δA_{12}, δA_{22}, and δJ instead of just the modulus of the transformation as was the case for conformal mapping. Therefore, to construct δI, an independent basis space of perturbation functions b_i, $i = 1, 2, \ldots, n$ (n = number of design variables) is chosen that allows for the needed freedom of the design space. Thus, the shape $\mathcal{F}$ now becomes $\mathcal{F}(b_i)$, where the functions b_i now represent the control. The variations δA_{11}, δA_{12}, δA_{22}, and δJ are obtained by a direct finite difference procedure with respect to each design variable b_i. Once δI is obtained, any optimization procedure can be employed to minimize the cost with respect to the given basis b_i.

If the flow is subsonic, this procedure should converge toward the desired speed distribution since the solution will remain smooth, and no unbounded derivatives will appear. If, however, the flow is transonic, one must allow for the appearance of shock waves in the trial solutions, even if q_d is smooth. In such instances $q - q_d$ is not differentiable. As in section 2, the cost function is redefined as

$$I = \frac{1}{2} \int_C \left(\lambda_1 \mathcal{Z}^2 + \lambda_2 \left(\frac{d\mathcal{Z}}{d\xi}\right)^2 \right) d\xi,$$

where λ_1 and λ_2 are parameters, and the periodic function $\mathcal{Z}(\xi)$ satisfies the equation

$$\lambda_1 \mathcal{Z} - \lambda_2 \frac{d^2 \mathcal{Z}}{d\xi^2} = q - q_d. \quad (42)$$

Then,

$$\delta I = \int_C \left(\lambda_1 \mathcal{Z} \delta \mathcal{Z} + \lambda_2 \frac{d\mathcal{Z}}{d\xi} \frac{d}{d\xi} \delta \mathcal{Z} \right) d\xi$$

$$= \int_C \mathcal{Z} \left(\lambda_1 \delta \mathcal{Z} - \lambda_2 \frac{d^2}{d\xi^2} \delta \mathcal{Z} \right) d\xi = \int_C \mathcal{Z} \delta q \, d\xi.$$

Thus, $\mathcal{Z}$ replaces $q - q_d$ in the previous formula and one modifies the boundary condition (40) to

$$\rho J \left(A_{12} \psi_\xi + A_{22} \phi_\eta \right) = -\frac{\partial}{\partial \xi} (\mathcal{Z}) \quad \text{on } C. \quad (43)$$

For the case where the cost function is drag, (34) is replaced by,

$$I = \int_C p \frac{\partial y}{\partial \xi} d\xi. \quad (44)$$

The first variation of the cost function is now,

$$\delta I = \int_C \delta p \frac{\partial y}{\partial \xi} d\xi + \int_C p \delta \left(\frac{\partial y}{\partial \xi}\right) d\xi$$

$$= \int_C \frac{\partial \left(\rho q \frac{\partial y}{\partial s} \right)}{\partial \xi} \delta \phi \, d\xi - \int_C \rho q \frac{\partial \phi}{\partial \xi} \frac{\partial y}{\partial \xi} \delta \left(\frac{\partial \xi}{\partial s}\right) d\xi$$

$$+ \int_C p \delta \left(\frac{\partial y}{\partial \xi}\right) d\xi. \quad (45)$$

8

Thus, (41) becomes

$$
\begin{aligned}
\delta I = \ & - \int_C \rho q \frac{\partial \phi}{\partial \xi} \frac{\partial y}{\partial \xi} \delta \left(\frac{\partial \xi}{\partial s} \right) d\xi \\
& + \int_C p \delta \left(\frac{\partial y}{\partial \xi} \right) d\xi \\
& + \int_D \frac{\partial \psi}{\partial \xi} Q + \frac{\partial \psi}{\partial \eta} P \ d\xi d\eta,
\end{aligned}
\tag{46}
$$

where the boundary condition on ψ, (40) or (42), is replaced with

$$
\rho J \left(A_{12} \psi_\xi + A_{22} \phi_\eta \right) = -\frac{\partial}{\partial \xi} \left(\rho q \frac{\partial y}{\partial s} \right)
\tag{47}
$$

or

$$
\lambda_1 \mathcal{Z} - \lambda_2 \frac{d^2 \mathcal{Z}}{d\xi^2} = \rho q \frac{\partial y}{\partial s}.
\tag{48}
$$

The entire procedure can be summarized for the cost function based on target speed distribution as follows:

1. Solve the flow equations (29–33) for ϕ, u, v, q, ρ, U, and V.

2. Smooth the cost function if necessary by (42).

3. Solve the adjoint equation (37 and 39) for ψ subject to the boundary condition (40) or (43).

4. For each i independently perturb the design variables, b_i, and calculate the necessary metric variations (δA_{11}, δA_{12}, δA_{22}, δJ, and $\delta \left(\frac{ds}{d\xi} \right)$) by recalculating the perturbed grid with automatic grid generation.

5. Directly evaluate δI by equation (41).

6. Project δI into a feasible direction subject to any constraints to obtain $\delta \tilde{I}$.

7. Feed $\delta \tilde{I}$ as the gradient with respect to b_i to a quasi-Newton optimization procedure.

8. Calculate the search direction with a quasi-Newton algorithm and perform a line search.

9. Return to 1 if the process has not converged.

In practice the method resembles that used by Hicks *et al.* [17] with the control theory replacing the brute force, finite difference based, gradient calculation. The current formulation has an advantage by requiring computational work proportional to $2 + m$ flow solver evaluations (m being the number of calculations required per line search) per design cycle as opposed to $1 + m + n$. Thus, unlike conventional design optimization programs, the current method's computational cost does not hinge upon the number of design variables provided the grid regeneration is fast and automatic. The method also has the advantage of being quite general, allowing arbitrary choices for both the design variables and the optimization technique.

5 NUMERICAL IMPLEMENTATION OF THE GENERALIZED POTENTIAL FLOW DESIGN METHOD

The practical implementation of the generalized potential flow design method, as with the conformal potential method, relies heavily upon fast accurate solvers for both the state (ϕ) and co-state (ψ) fields. Further, to improve the speed and realizability of the methods, a robust choice of the optimization algorithm must be made. Finally, appropriate design variables must be chosen which allow sufficient freedom in realizable designs. In this work, the author's FLO42 full potential computer program and the QNMDIF (by Gill, Murray and Wright [4]) quasi-Newton optimization algorithm are employed.

In FLO42 the flow solution is obtained by a rapid multigrid alternating direction method [7]. The scheme uses artificial dissipative terms to introduce upwind biasing which simulates the rotated difference scheme [6] while preserving the conservation form. The alternating direction method is a generalization of conventional alternating direction methods in which the scalar parameters are replaced by upwind difference operators to produce a scheme which remains stable as the equations change type from elliptic to hyperbolic in accordance with the flow becoming locally supersonic [7].

QNMDIF is an unconstrained quasi-Newton optimization algorithm that calculates updates to a Cholesky factored Hessian matrix by the BFGS (Broyden-Fletcher-Goldfarb-Shanno) rank-two procedure. Hence, information about the curvature of the design space feeds in through the successive gradient calculations.

Since the primary computational costs arise from not only the flow solution algorithm but also the adjoint solution algorithm, both need to be computationally efficient. The adjoint equation has a form very similar to the flow equation. While it is linear in its dependent variable, it also changes type from elliptic (in subsonic zones of the flow) to hyperbolic (in supersonic zones of the flow). Thus, it was possible to adapt exactly the same algorithm to solve both the adjoint and the flow equations, but with reverse biasing of the difference operators in the downwind direction for the adjoint equation, corresponding to its reversed direction of the zone of dependence. A multigrid method is used to accelerate the convergence of a generalized alterating direction scheme in a manner similar to the flow solver.

Design variables are chosen with the following form, suggested by Hicks and Henne [5]:

$$
b(x) = \sin \left(\pi x^{\frac{\log_{10}(.5)}{\log_{10}(t_1)}} \right)^{t_2}
$$

$$
b(x) = x^{t_1} (1 - x) e^{-t_2 x},
$$

where t_1 and t_2 control the center and thickness of the perturbation and x is the normalized chord length. When distributed over the entire chord on both upper and lower surfaces these analytic perturbation functions admit a large

possible design space. They have the advantage of being space based functions, as opposed to frequency based functions, and thus they allow for local control of the design. They can be chosen such that symmetry, thickness, or volume can be explicitly constrained. Further, particular choices of these variables will concentrate the design effort in regions where refinement is needed, while leaving the rest of the airfoil section virtually undisturbed. The disadvantage of these functions is that they do not form a complete basis space, nor are they orthogonal. Thus, they do not guarantee that a solution, for example, of the inverse problem for a realizable target pressure distribution will necessarily be attained. Here they are employed due to their ease of use and ability to produce a wide variation of shapes with a limited number of design variables.

The generalized potential flow design algorithm based on the finite volume scheme has been applied to a variety of test cases, which are described in the following paragraphs. These include both non-lifting cases, where a symmetric target pressure distribution is specified and the optimization is started from an arbitrary symmetric initial guess, and lifting cases where the target pressure distribution is specified, and finally cases which verify the capability of the method to find profiles with minimum drag.

The first non-lifting example shown in Figure 4, illustrates that for subsonic flow, $M_\infty = 0.2$ and $\alpha = 0°$, a given airfoil shape, in this case a NACA 64012, can be recovered by starting from an arbitrary shape and specifying the target pressure distribution. A close look at the final solution shows that a small discrepancy is evident at the trailing edge. This may be associated with the lack of completeness of our basis space. In the next example, see Figure 5, the design takes place at $M_\infty = 0.8$, $\alpha = 0°$, where the initial NACA 0012 airfoil is driven towards the subsonic pressure distribution of the NACA 64021. In this case the target pressure distribution exceeds Cp^* for $M_\infty = 0.8$. Therefore, the pressure distribution represents shock free transonic flow. Since, in general, such a pressure distribution may not be realizable, the program approaches the target with the nearest feasible pressure distribution. An examination of Figure 5 demonstrates that a very weak shock in the designed pressure distribution replaces the smooth transition to subsonic flow seen in the target distribution. In the final example non-lifting case of Figure 6, an arbitrary pressure distribution which does contain a shock wave and is realizable, is used as the target. Here the computer program was able to obtain the corresponding airfoil geometry along with the correct shock wave location with a high degree of accuracy, as can be seen both in the pressure distribution and in the airfoils.

The second group of test cases address the problem of attaining a desired pressure distribution for lifting airfoils. The most convenient method of obtaining such solutions with the present design method is to determine the lift coefficient associated with the target pressure distribution,

and match this lift with the initial airfoil. The design progresses with the flow solver and the adjoint system being driven by constant circulation instead of fixed angle of attack. The first example using this technique, shown in Figure 7, drives the NACA 0012 airfoil toward the target pressure distribution for the NACA 64A410 airfoil at $M_\infty = 0.735$, $\alpha = 0°$, and $C_l = 0.75$. This case requires a shift in the shock location and a significant change in the profile shape such that the target pressure distribution is obtained. The final solution almost exactly recovers the pressure distribution and the airfoil shape. In the next example, Figure 8, the NACA 0012 airfoil is again used as the starting condition to obtain the pressure distribution of the GAW72 airfoil operating at $M_\infty = 0.7$, $\alpha = -2°$, and $C_l = 0.57$. This case is difficult since the target airfoil has a cusped trailing edge while the initial airfoil has a finite trailing edge. As was seen in some of the non-lifting cases, there are small discrepancies evident near the trailing edge that may be due to the incomplete basis of the chosen design variables. The difference in the profiles between the final design and actual GAW72 is partly due to the fact that the GAW72 coordinates place the trailing edge at a non-zero y ordinate while the NACA 0012 places the trailing edge at $y = 0$. Also, the redesigned airfoil is subject to an arbitrary rotation since the angle of attack is free during optimization. The last test case in which the design program is run in inverse mode involves driving the NACA 0012 airfoil at $M_\infty = 0.75$ to obtain the target pressure distribution of the RAE airfoil at the same Mach number, $\alpha = 1.0°$, and $C_l = 0.80$. Due to the steep favorable pressure gradient at the leading edge upper surface and the strong shock exhibited (see Figure 9) by the RAE airfoil at these conditions this case represents quite a difficult test for the program. The method recovers the target pressure distribution almost exactly. A comparison of the profiles reveals that the the designed airfoil has no observable differences when overlayed with the original airfoil.

The last group of results introduces drag as the cost function. Again the design process is carried out in the fixed lift mode. In Figure 10, the first drag minimization example, a NACA 0012 is again used as a starting airfoil. The design takes place at $M_\infty = 0.75$ and $C_l = 0.50$ where a strong shock causes considerable wave drag in the initial airfoil. To make the problem interesting, the optimization is carried out such that symmetry of the design is preserved. The final design is a symmetric airfoil with an increased maximum thickness that operates at the same lift coefficient, but has a reduction in drag from $C_d = 0.0127$ to $C_d = 0.0016$. In the final test case (see Figure 9) the camber distribution is optimized instead of thickness distribution. The design starts from a NACA 64A410 airfoil operating at $M_\infty = 0.75$, and $C_l = 0.60$ which displays 42 counts of drag according to the potential flow calculation. By allowing only changes to the camber distribution, a final airfoil is produced which maintains $C_l = 0.60$ but does so with only 4 counts of drag.

6 DESIGN OF AIRFOILS USING THE EULER EQUATIONS

This section extends the application of control theory for aerodynamic shape optimization to the Euler equations for two dimensional flow. Consider the case of compressible flow over an airfoil. In the absence of separation and other strong viscous effects, the flow is well approximated by the Euler equations. In contrast to the previous implementations which relied on the isentropic potential equation, here strong inviscid shocks are modeled correctly with entropy production. Consider the flow in a domain D. The profile defines the inner boundary C, while the outer boundary B is assumed to be distant from the profile. Let p, ρ, u, v, E and H denote the pressure, density, Cartesian velocity components, total energy and total enthalpy. For a perfect gas

$$p = (\gamma - 1)\rho \left\{ E - \frac{1}{2} \left(u^2 + v^2 \right) \right\}, \qquad (49)$$

and

$$\rho H = \rho E + p, \qquad (50)$$

where γ is the ratio of the specific heats. The Euler equations may then be written as

$$\frac{\partial w}{\partial t} + \frac{\partial f}{\partial x} + \frac{\partial g}{\partial y} = 0 \quad \text{in } D, \qquad (51)$$

where x and y are Cartesian coordinates, t is the time coordinate and

$$w = \left\{ \begin{array}{c} \rho \\ \rho u \\ \rho v \\ \rho E \end{array} \right\},$$

$$f = \left\{ \begin{array}{c} \rho u \\ \rho u^2 + p \\ \rho u v \\ \rho u H \end{array} \right\}, \quad g = \left\{ \begin{array}{c} \rho v \\ \rho v u \\ \rho v^2 + p \\ \rho v H \end{array} \right\}. \qquad (52)$$

Consider a coordinate transformations to computational coordinates ξ, η with the transformation matrix

$$K = \left[\begin{array}{cc} \frac{\partial x}{\partial \xi} & \frac{\partial x}{\partial \eta} \\ \frac{\partial y}{\partial \xi} & \frac{\partial y}{\partial \eta} \end{array} \right],$$

and the Jacobian

$$J = \frac{\partial x}{\partial \xi} \frac{\partial y}{\partial \eta} - \frac{\partial x}{\partial \eta} \frac{\partial y}{\partial \xi}.$$

Introduce contravariant velocity components

$$\left\{ \begin{array}{c} U \\ V \end{array} \right\} = K^{-1} \left\{ \begin{array}{c} u \\ v \end{array} \right\} = \frac{1}{J} \left[\begin{array}{cc} \frac{\partial y}{\partial \eta} & -\frac{\partial x}{\partial \eta} \\ -\frac{\partial y}{\partial \xi} & \frac{\partial x}{\partial \xi} \end{array} \right] \left\{ \begin{array}{c} u \\ v \end{array} \right\}.$$

The Euler equations can be written as

$$\frac{\partial W}{\partial t} + \frac{\partial F}{\partial \xi} + \frac{\partial G}{\partial \eta} = 0 \quad \text{in } D, \qquad (53)$$

with

$$W = J \left\{ \begin{array}{c} \rho \\ \rho u \\ \rho v \\ \rho E \end{array} \right\},$$

$$F = J \left\{ \begin{array}{c} \rho U \\ \rho U u + \frac{\partial \xi}{\partial x} p \\ \rho U v + \frac{\partial \xi}{\partial y} p \\ \rho U H \end{array} \right\}, \quad G = J \left\{ \begin{array}{c} \rho V \\ \rho V u + \frac{\partial \eta}{\partial x} p \\ \rho V v + \frac{\partial \eta}{\partial y} p \\ \rho V H \end{array} \right\}. \qquad (54)$$

Assume now that the computational coordinate system conforms to the airfoil section in such a way that the surface C is represented by $\eta = 0$. Then the flow is determined as the steady state solution of the equation (54) subject to the flow tangency condition

$$V = 0 \quad \text{on } C, \qquad (55)$$

At the far field boundary B, conditions are specified for incoming waves, while outgoing waves are determined by the solution.

Consider the case of the inverse problem where the cost function may be defined as

$$I = \frac{1}{2} \int_C (p - p_d)^2 \, ds = \frac{1}{2} \int_C (p - p_d)^2 \left(\frac{ds}{d\xi} \right) d\xi,$$

where p_d is the desired pressure. The design problem is now treated as a control problem where the control function is the airfoil shape, which is to be chosen to minimize I subject to the constraints defined by the flow equations (53–55). A variation in the shape will cause a variation δp in the pressure in addition to a variation in the geometry and consequently the variation in the cost function becomes

$$\begin{aligned} \delta I &= \int_C (p - p_d) \delta p \left(\frac{ds}{d\xi} \right) d\xi \\ &\quad + \frac{1}{2} \int_C (p - p_d)^2 \delta \left(\frac{ds}{d\xi} \right) d\xi. \qquad (56) \end{aligned}$$

Since p depends on w through the equation of state (51–52), the variation δp can be determined from the variation δw. Define the Jacobian matrices

$$A_1 = \frac{\partial f}{\partial w}, \quad A_2 = \frac{\partial g}{\partial w}, \quad C_i = \sum_j J K_{ij}^{-1} A_j. \qquad (57)$$

Then the equation for δw in the steady state becomes

$$\frac{\partial}{\partial \xi} (\delta F) + \frac{\partial}{\partial \eta} (\delta G) = 0, \qquad (58)$$

where

$$\delta F = C_1 \delta w + \delta \left(J \frac{\partial \xi}{\partial x} \right) f + \delta \left(J \frac{\partial \xi}{\partial y} \right) g$$

$$\delta G = C_2 \delta w + \delta \left(J \frac{\partial \eta}{\partial x} \right) f + \delta \left(J \frac{\partial \eta}{\partial y} \right) g.$$

Now, multiplying by a vector co-state variable ψ and integrating over the domain

$$\int_D \psi^T \left(\frac{\partial \delta F}{\partial \xi} + \frac{\partial \delta G}{\partial \eta} \right) d\xi d\eta = 0,$$

and if ψ is differentiable this may be integrated by parts to give

$$\int_D \left(\frac{\partial \psi^T}{\partial \xi} \delta F + \frac{\partial \psi^T}{\partial \eta} \delta G \right) d\xi d\eta =$$
$$\int_B \left(n_1 \psi^T \delta F + n_2 \psi^T \delta G \right) d\xi$$
$$+ \int_C \left(n_1 \psi^T \delta F + n_2 \psi^T \delta G \right) d\xi,$$

where n_i are the components of a unit vector normal to the boundary. No boundary integrals appear in the η direction because the mesh is assumed to be of O-type, with the result that the solution is periodic in the ξ coordinate thereby canceling the η boundary integrals. Thus the variation in the cost function may now be written

$$\delta I = \int_C (p - p_d) \delta p \left(\frac{ds}{d\xi} \right) d\xi$$
$$+ \frac{1}{2} \int_C (p - p_d)^2 \delta \left(\frac{ds}{d\xi} \right) d\xi$$
$$+ \int_D \left(\frac{\partial \psi^T}{\partial \xi} \delta F + \frac{\partial \psi^T}{\partial \eta} \delta G \right) d\xi d\eta$$
$$- \int_B \left(n_1 \psi^T \delta F + n_2 \psi^T \delta G \right) d\xi$$
$$- \int_C \left(n_1 \psi^T \delta F + n_2 \psi^T \delta G \right) d\xi.$$

On the profile $n_1 = 0$ and $n_2 = -1$. It follows from equation (55) that

$$\delta G = J \left\{ \begin{array}{c} 0 \\ \frac{\partial \eta}{\partial x} \delta p \\ \frac{\partial \eta}{\partial y} \delta p \\ 0 \end{array} \right\} + p \left\{ \begin{array}{c} 0 \\ \delta \left(J \frac{\partial \eta}{\partial x} \right) \\ \delta \left(J \frac{\partial \eta}{\partial y} \right) \\ 0 \end{array} \right\}. \quad (59)$$

Suppose now that ψ is the steady state solution of the adjoint equation

$$\frac{\partial \psi}{\partial t} - C_1^T \frac{\partial \psi}{\partial \xi} - C_2^T \frac{\partial \psi}{\partial \eta} = 0 \quad \text{in } D. \quad (60)$$

At the outer boundary incoming characteristics for ψ correspond to outgoing characteristics for δw. Consequently, one can choose boundary conditions for ψ such that

$$n_i \psi^T C_i \delta w = 0.$$

Then if the coordinate transformation is such that $\delta \left(J K^{-1} \right)$ is negligible in the far field, the only remaining boundary term is

$$\int_C \psi^T \delta G d\xi.$$

Thus by letting ψ satisfy the boundary condition,

$$J \left(\psi_2 \frac{\partial \eta}{\partial x} + \psi_3 \frac{\partial \eta}{\partial y} \right) = - (p - p_d) \frac{ds}{d\xi} \quad \text{on } C, \quad (61)$$

we find finally that

$$\delta I = \frac{1}{2} \int_C (p - p_d)^2 \delta \left(\frac{ds}{d\xi} \right) d\xi$$
$$+ \int_D \frac{\partial \psi^T}{\partial \xi} \left(\delta \left(J \frac{\partial \xi}{\partial x} \right) f + \delta \left(J \frac{\partial \xi}{\partial y} \right) g \right) d\xi d\eta$$
$$+ \int_D \frac{\partial \psi^T}{\partial \eta} \left(\delta \left(J \frac{\partial \eta}{\partial x} \right) f + \delta \left(J \frac{\partial \eta}{\partial y} \right) g \right) d\xi d\eta$$
$$+ \int_C \left\{ \psi_2 \delta \left(J \frac{\partial \eta}{\partial x} \right) + \psi_3 \delta \left(J \frac{\partial \eta}{\partial y} \right) \right\} p d\xi. \quad (62)$$

If the flow is subsonic, this procedure should converge toward the desired pressure distribution since the solution will remain smooth, and no unbounded derivatives will appear. If, however, the flow is transonic, one must allow for the appearance of shock waves in the trial solutions, even if p_d is smooth. In such instances $p - p_d$ is not differentiable. As in the case of potential flow, this difficulty can be circumvented by a more sophisticated choice of the cost function. Consider the choice

$$I = \frac{1}{2} \int_C \left(\lambda_1 Z^2 + \lambda_2 \left(\frac{dZ}{d\xi} \right)^2 \right) \frac{ds}{d\xi} d\xi,$$

where λ_1 and λ_2 are parameters, and the periodic function $Z(\xi)$ satisfies the equation

$$\lambda_1 Z - \lambda_2 \frac{d^2 Z}{d\xi^2} = p - p_d. \quad (63)$$

Then,

$$\delta I = \int_C \left(\lambda_1 Z \delta Z + \lambda_2 \frac{dZ}{d\xi} \frac{d}{d\xi} \delta Z \right) \frac{ds}{d\xi} d\xi$$
$$= \int_C Z \left(\lambda_1 \delta Z - \lambda_2 \frac{d^2}{d\xi^2} \delta Z \right) \frac{ds}{d\xi} d\xi$$
$$= \int_C Z \delta q \frac{ds}{d\xi} d\xi.$$

Thus, Z replaces $p - p_d$ with a corresponding modification to the boundary condition for the adjoint equations.

A convenient way to treat an airfoil is to use a conformal mapping of the profile in the z plane to a near circle in the σ plane, followed by shearing of the radial coordinate to make the system boundary conforming. Polar coordinates are introduced in the mapped plane σ. When mapped back to the physical plane this gives a smooth,

nearly orthogonal grid. This procedure is intermediate between the use of a full conformal mapping as in section 2 and an arbitrary numerically generated grid as in section 4. We can now specialize our generalized design procedure to treat this grid system. Define the first conformal mapping from z to σ by letting the derivative of the mapping function be

$$\frac{dz}{d\sigma} = h e^{i\beta}.$$

Now using polar coordinates r, and θ in the σ plane, the first transformation matrix is

$$K_1 = \left[\begin{array}{cc} x_\theta & x_r \\ y_\theta & y_r \end{array} \right] = h \left[\begin{array}{cc} rs & c \\ -cs & s \end{array} \right],$$

and we can define contravariant velocities

$$\left\{ \begin{array}{c} U \\ V \end{array} \right\} = \left[\begin{array}{cc} s & -c \\ c & s \end{array} \right] \left\{ \begin{array}{c} u \\ v \end{array} \right\},$$

where

$$s = \sin(\beta - \theta), \quad c = \cos(\beta - \theta).$$

The Euler equations can now be represented in the σ plane as

$$\frac{\partial (rh^2 W)}{\partial t} + \frac{\partial (hF)}{\partial \theta} + \frac{\partial (rhG)}{\partial r} = 0 \quad \text{in } D, \quad (64)$$

where

$$W = \left\{ \begin{array}{c} \rho \\ \rho u \\ \rho v \\ \rho E \end{array} \right\},$$

$$F = \left\{ \begin{array}{c} \rho U \\ \rho U u + sp \\ \rho U v - cp \\ \rho U H \end{array} \right\}, \quad G = \left\{ \begin{array}{c} \rho V \\ \rho V u + cp \\ \rho V v + sp \\ \rho V H \end{array} \right\}.$$

$$(65)$$

Now let the final computational coordinates be defined by a radial shearing transformation

$$\theta = \xi, \quad r = \eta + S(\xi)$$

and the transformation matrix

$$K_2 = \left[\begin{array}{cc} \frac{\partial \theta}{\partial \xi} & \frac{\partial \theta}{\partial \eta} \\ \frac{\partial r}{\partial \xi} & \frac{\partial r}{\partial \eta} \end{array} \right] = \left[\begin{array}{cc} 1 & 0 \\ \frac{\partial S}{\partial \xi} & 1 \end{array} \right], \quad \det(K_2) = 1.$$

Now we can identify the complete transformation matrix as

$$K = K_1 K_2 = h \left[\begin{array}{cc} rs + S_\xi c & c \\ -rc + S_\xi s & s \end{array} \right],$$

while the fluxes are

$$\begin{array}{rcl} hF & = & h(sf - cg) \\ & = & y_\eta f - x_\eta g \end{array}$$

and

$$\begin{array}{rcl} h\left[(\eta + S)G - S_\xi F\right] & = & h\left[(\eta + S)c - S_\xi s\right] f \\ & + & h\left[(\eta + S)s + S_\xi c\right] g \\ & = & x_\xi g - y_\xi f. \end{array}$$

Thus the Euler equations assume the form

$$\frac{\partial}{\partial t}\left((\eta + S)h^2 W\right)$$
$$+ \frac{\partial}{\partial \xi}(hF) + \frac{\partial}{\partial \eta}\left(h(\eta + S)G - hS_\xi F\right) = 0,$$

while the surface tangency condition on the velocity becomes

$$x_\xi v - y_\xi u = h\left[(\eta + S)V - S_\xi U\right] = 0.$$

Now we take $S(\xi)$ as the control. It is also convenient to represent the inverse problem by the cost function

$$I = \frac{1}{2}\int_C (p - p_d)^2 \, d\theta = I = \frac{1}{2}\int_C (p - p_d)^2 \, d\xi.$$

This eliminates terms in $\delta\left(\frac{ds}{d\xi}\right)$ from the gradient. The variations in the fluxes become

$$\begin{array}{rcl} \delta(hF) & = & C_1 \delta w \\ \delta\left[h(\eta + S)G - hS_\xi F\right] & = & C_2 \delta w + h\delta S G - h\delta S_\xi F \end{array}$$

where C_1 and C_2 are the Jacobian matrices defined in equation (57). Choosing ψ to satisfy the adjoint equation (60) with the boundary condition

$$x_\xi \psi_3 - y_\xi \psi_2 = h\left[(\eta + S)s + S_\xi c\right] \psi_\eta = p - p_d$$

the variation in the cost reduces to

$$\begin{array}{rcl} \delta I & = & \displaystyle\int_C (p - p_d)\delta p \, d\xi \\ & + & \displaystyle\int_D \psi^T \left(\frac{\partial}{\partial \xi}\delta F + \frac{\partial}{\partial \eta}\delta G\right) d\xi \, d\eta \\ & = & \displaystyle\int_C \psi^T \left(\delta S h\bar{G} - \delta S_\xi h\bar{F}\right) d\xi \\ & + & \displaystyle\int_D \psi^T \frac{\partial}{\partial \xi}\left(\delta S \, hG + \delta S_\xi \, hF\right) d\xi \, d\eta, \end{array}$$

where F and G are the fluxes defined in equation (65), and $\bar{F}$ and $\bar{G}$ are F and G with the pressure terms deleted. Define

$$\begin{array}{rcl} P & = & \psi^T h\bar{F} + \displaystyle\int \psi^T \frac{\partial}{\partial \eta}(hF) \, d\eta \\ Q & = & \psi^T h\bar{G} + \displaystyle\int \psi^T \frac{\partial}{\partial \eta}(hG) \, d\eta. \end{array}$$

13

Then

$$
\begin{aligned}
\delta I &= \int_C \left(Q\delta S - P\delta S_\xi\right) d\xi \\
&= \int_C \mathcal{G}\delta S d\xi,
\end{aligned}
$$

where the gradient is

$$
\mathcal{G} = Q + \frac{\partial P}{\partial \xi}. \tag{66}
$$

The entire procedure can be summarized as follows.

1. Solve the flow equations (51–55) for ρ, u, v, p, E, H, U, and V.

2. Smooth the cost function if necessary by (63).

3. Solve the adjoint equations (60) for ψ subject to the boundary condition (61).

4. Calculate P and Q from the variation in the control $S(\xi)$.

5. Evaluate $\mathcal{G}$ by equation (66)

6. Project $\mathcal{G}$ into a feasible direction subject to any constraints to obtain $\bar{\mathcal{G}}$.

7. Correct the mapping in the direction of steepest decent

$$
\delta S(\xi) = -\lambda\bar{\mathcal{G}}.
$$

or by using $\bar{\mathcal{G}}$ as the gradient in a quasi-Newton or conjugate gradient search method.

8. Return to 1.

7 IMPLEMENTATION OF THE EULER BASED DESIGN METHOD

The practical implementation of design method relies heavily upon fast accurate solvers for both the state (w) and co-state (ψ) fields. Further, to improve the speed and realizability of the method, a robust choice of the optimization algorithm must be made. In this work, the author's FLO82 full computer program has been used to solve the Euler equations. This program uses a multi stage time stepping scheme with multi grid acceleration to obtain very rapid steady state solutions, typically in 25 steps [8, 9]. The adjoint equations are solved by a similar method, in which the flux calculations for the Euler equations are replaced by the corresponding formulas for the adjoint equation.

In the initial tests a simple gradient procedure has been used as the optimization process. To preserve the smoothness of the profile the gradient is smoothed at each step in a similar manner to that used in the method of

section 2. Thus the change in the shape function $S(\xi)$ is defined by solving

$$
\delta S - \frac{\partial}{\partial \xi}\beta\frac{\partial}{\partial \xi}\delta S = -\lambda\mathcal{G},
$$

where β is a smoothing parameter. Then, to first order, the variation in the cost is

$$
\begin{aligned}
\delta I &= \int \mathcal{G}\delta S d\xi \\
&= -\int \frac{1}{\lambda}\left[\delta S - \delta S\frac{\partial}{\partial \xi}\beta\frac{\partial}{\partial \xi}\delta S\right] d\xi \\
&= -\int \frac{1}{\lambda}\left[\delta S^2 + \beta\left(\frac{\partial}{\partial \xi}\delta S\right)^2\right] d\xi \\
&< 0.
\end{aligned}
$$

The option to minimize the pressure drag coefficient

$$
I = C_d = \frac{1}{\frac{1}{2}\rho_\infty q_\infty^2 \bar{c}}\int_C p\frac{\partial y}{\partial \xi}d\xi,
$$

where $\bar{c}$ is the chord length, has also been included. To prevent the procedure from trying to reduce drag by reducing the profile to a non-lifting flat plate a target pressure distribution is retained in the cost function, which becomes

$$
I = \frac{1}{2}\Omega_1 \int_C (p - p_d)^2 d\xi + \Omega_2 C_d
$$

where Ω_1 and Ω_2 are weighting parameters. Also the calculations are performed at a fixed lift coefficient corresponding to that of the target pressure distribution, while the angle of attack is allowed to vary as needed. Three test cases are presented for the design algorithm. The first two address the problem of attaining a desired pressure distribution. The first example using this technique, shown in Figure 12, drives the Korn airfoil toward the target pressure distribution for the NACA 64A410 airfoil at $M_\infty = 0.75$, $\alpha = 0°$, and $C_l = 0.7$. This case requires a shift in the shock location and a significant change in the profile shape such that the target pressure distribution is obtained. The final solution almost exactly recovers the pressure distribution and the airfoil shape. In the next example, Figure 13, the Korn airfoil operating at $M_\infty = 0.78$ is used as the starting condition to obtain the pressure distribution of the same airfoil operating at $M_\infty = 0.75$, $\alpha = 0°$, and $C_l = 0.64$. This case is difficult since the target pressure distribution may not be realizable from a physical profile. Note that while the achieved pressure distribution is very close to the target pressure distribution, the drag of 77 counts is much larger then the zero drag experienced by the Korn airfoil at its design point. The third test case introduces drag as the cost function. Again the design process is carried out in the fixed lift mode. In Figure 14, a NACA 64A410 is again used as a starting airfoil. The design takes place at

14

$M_\infty = 0.75$ and $C_l = 0.68$ where a strong shock causes considerable wave drag in the initial airfoil. To preserve a reasonable lifting airfoil shape the cost function is constructed as a blend of preserving the original pressure distribution and reducing the drag. The final design has a reduction in drag from $C_d = 0.0144$ to $C_d = 0.0018$.

8 THREE DIMENSIONAL DESIGN USING THE EULER EQUATIONS

In order to illustrate further the application of control theory to aerodynamic design problems, sections 8 and 9 treat the case of three-dimensional wing design, again using the inviscid Euler equations as the mathematical model for compressible flow. In this case it proves convenient to denote the Cartesian coordinates and velocity components by x_1, x_2, x_3 and u_1, u_2, u_3, and to use the convention that summation over $i = 1$ to 3 is implied by a repeated index i. The three-dimensional Euler equations may be written as

$$\frac{\partial w}{\partial t} + \frac{\partial f_i}{\partial x_i} = 0 \quad \text{in } D, \qquad (67)$$

where

$$w = \left\{ \begin{array}{c} \rho \\ \rho u_1 \\ \rho u_2 \\ \rho u_3 \\ \rho E \end{array} \right\}, \quad f_i = \left\{ \begin{array}{c} \rho u_i \\ \rho u_i u_1 + p\delta_{i1} \\ \rho u_i u_2 + p\delta_{i2} \\ \rho u_i u_3 + p\delta_{i3} \\ \rho u_i H \end{array} \right\} \qquad (68)$$

and δ_{ij} is the Kronecker delta function. Also,

$$p = (\gamma - 1)\rho \left\{ E - \frac{1}{2} \left(u_i^2 \right) \right\}, \qquad (69)$$

and

$$\rho H = \rho E + p \qquad (70)$$

where γ is the ratio of the specific heats. Consider a transformation to coordinates ξ_1, ξ_2, ξ_3 where

$$K_{ij} = \left[\frac{\partial x_i}{\partial \xi_j} \right], \quad J = \det(K), \quad K_{ij}^{-1} = \left[\frac{\partial \xi_i}{\partial x_j} \right].$$

Introduce contravariant velocity components as

$$\left\{ \begin{array}{c} U_1 \\ U_2 \\ U_3 \end{array} \right\} = K^{-1} \left\{ \begin{array}{c} u_1 \\ u_2 \\ u_3 \end{array} \right\}$$

The Euler equations can now be written as

$$\frac{\partial W}{\partial t} + \frac{\partial F_i}{\partial \xi_i} = 0 \quad \text{in } D, \qquad (71)$$

with

$$W = J \left\{ \begin{array}{c} \rho \\ \rho u_1 \\ \rho u_2 \\ \rho u_3 \\ \rho E \end{array} \right\}, \quad F_i = J \left\{ \begin{array}{c} \rho U_i \\ \rho U_i u_1 + \frac{\partial \xi_i}{\partial x_1} p \\ \rho U_i u_2 + \frac{\partial \xi_i}{\partial x_2} p \\ \rho U_i u_3 + \frac{\partial \xi_i}{\partial x_3} p \\ \rho U_i H \end{array} \right\}. \qquad (72)$$

Assume now that the new computational coordinate system conforms to the wing in such a way that the wing surface B_W is represented by $\xi_2 = 0$. Then the flow is determined as the steady state solution of equation (71) subject to the flow tangency condition

$$U_2 = 0 \quad \text{on } B_W. \qquad (73)$$

At the far field boundary B_F, conditions are specified for incoming waves, as in the two-dimensional case, while outgoing waves are determined by the solution.

Suppose now that it is desired to control the surface pressure by varying the wing shape. It is convenient to retain a fixed computational domain. Variations in the shape then result in corresponding variations in the mapping derivatives defined by H. Introduce the cost function

$$I = \frac{1}{2} \int\int_{B_W} (p - p_d)^2 \, d\xi_1 d\xi_3,$$

where p_d is the desired pressure. The design problem is now treated as a control problem where the control function is the wing shape, which is to be chosen to minimize I subject to the constraints defined by the flow equations (71–72). A variation in the shape will cause a variation δp in the pressure and consequently the a variation in the cost function

$$\delta I = \int\int_{B_W} (p - p_d)\delta p \, d\xi_1 d\xi_3. \qquad (74)$$

Since p depends on w through the equation of state (69–70), the variation δp can be determined from the variation δw. Define the Jacobian matrices

$$A_i = \frac{\partial f_i}{\partial w}, \quad C_i = JK_{ij}^{-1}A_j. \qquad (75)$$

Then the equation for δw in the steady state becomes

$$\frac{\partial}{\partial \xi_i}(\delta F_i) = 0, \qquad (76)$$

where

$$\delta F_i = C_i \delta w + \delta \left(J \frac{\partial \xi_i}{\partial x_j} \right) f_j.$$

Now, multiplying by a vector co-state variable ψ and integrating over the domain

$$\int_{D_j} \psi^T \left(\frac{\partial \delta F_i}{\partial \xi_i} \right) d\xi_j = 0,$$

and if ψ is differentiable this may be integrated by parts to give

$$\int_{D_j} \left(\frac{\partial \psi^T}{\partial \xi_i} \delta F_i \right) d\xi_j = \int_B \left(n_i \psi^T \delta F_i \right) d\xi_B,$$

where n_i are components of a unit vector normal to the boundary. Thus the variation in the cost function may

15

now be written

$$\delta I = \iint_{B_W} (p - p_d)\,\delta p \ d\xi_1 d\xi_3$$

$$- \int_{D_j} \left(\frac{\partial \psi^T}{\partial \xi_i} \delta F_i \right) d\xi_j$$

$$+ \int_B \left(n_i \psi^T \delta F_i \right) d\xi_B. \qquad (77)$$

On the wing surface B_W, $n_1 = n_3 = 0$ and it follows from equation (73) that

$$\delta F_2 = J \left\{ \begin{array}{c} 0 \\ \frac{\partial \xi_2}{\partial x_1} \delta p \\ \frac{\partial \xi_2}{\partial x_2} \delta p \\ \frac{\partial \xi_2}{\partial x_3} \delta p \\ 0 \end{array} \right\} + p \left\{ \begin{array}{c} 0 \\ \delta \left(J \frac{\partial \xi_2}{\partial x_1} \right) \\ \delta \left(J \frac{\partial \xi_2}{\partial x_2} \right) \\ \delta \left(J \frac{\partial \xi_2}{\partial x_3} \right) \\ 0 \end{array} \right\}. \qquad (78)$$

Suppose now that ψ is the steady state solution of the adjoint equation

$$\frac{\partial \psi}{\partial t} - C_i^T \frac{\partial \psi}{\partial \xi_i} = 0 \quad \text{in } D. \qquad (79)$$

At the outer boundary incoming characteristics for ψ correspond to outgoing characteristics for δw. Consequently, as in the two-dimensional case, one can choose boundary conditions for ψ such that

$$n_i \psi^T C_i \delta w = 0.$$

Then if the coordinate transformation is such that $\delta \left(J K^{-1} \right)$ is negligible in the far field, the only remaining boundary term is

$$- \iint_{B_W} \psi^T \delta F_2 \ d\xi_1 d\xi_3.$$

Thus by letting ψ satisfy the boundary condition,

$$J \left(\psi_2 \frac{\partial \xi_2}{\partial x_1} + \psi_3 \frac{\partial \xi_2}{\partial x_2} + \psi_4 \frac{\partial \xi_2}{\partial x_3} \right) = (p - p_d) \text{ on } B_W, \qquad (80)$$

we find finally that

$$\delta I = \int_D \frac{\partial \psi^T}{\partial \xi_i} \delta \left(J \frac{\partial \xi_i}{\partial x_j} \right) f_j d\xi_D$$

$$- \iint_{B_W} \left\{ \psi_2 \frac{\partial \xi_2}{\partial x_1} + \psi_3 \frac{\partial \xi_2}{\partial x_2} + \psi_4 \frac{\partial \xi_2}{\partial x_3} \right\} p \ d\xi_1 d\xi_3. \qquad (81)$$

A convenient way to treat a wing is to introduce sheared parabolic coordinates as shown in figure 2 through the transformation

$$\begin{aligned} x &= x_0(\zeta) + \frac{1}{2} a(\zeta) \left\{ \xi^2 - (\eta + S(\xi, \zeta))^2 \right\} \\ y &= y_0(\zeta) + a(\zeta) \xi (\eta + S(\xi, \zeta)) \\ z &= \zeta. \end{aligned}$$

2a: x, y-Plane.

2b: ξ, η-Plane.
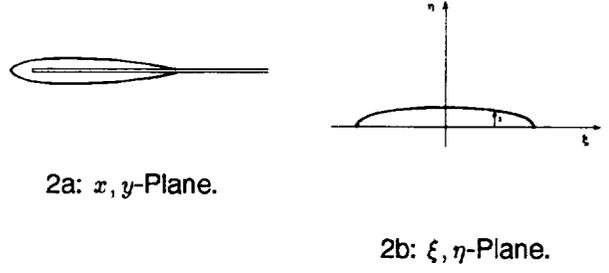
Figure 2: Sheared Parabolic Mapping.

Here $x = x_1$, $y = x_2$, $z = x_3$ are the Cartesian coordinates, and ξ and $\eta + S$ correspond to parabolic coordinates generated by the mapping

$$x + iy = x_0 + iy_0 + \frac{1}{2} a(\zeta) \left\{ \xi + i(\eta + S) \right\}^2$$

at a fixed span station ζ. $x_0(\zeta)$ and $y_0(\zeta)$ are the coordinates of a singular line which is swept to lie just inside the leading edge of a swept wing, while $a(\zeta)$ is a scale factor to allow for spanwise chord variations. The surface $\eta = 0$ is a shallow bump corresponding to the wing surface, with a height $S(\xi, \zeta)$ determined by the equation

$$\xi + iS = \sqrt{2 \left(x_{B_W} + iy_{B_W} \right)},$$

where $x_{B_W}(z)$ and $y_{B_W}(z)$ are coordinates of points lying on the wing surface. We now treat $S(\xi, \zeta)$ as the control.

In this case the transformation matrix $\frac{\partial x_i}{\partial \xi_j}$ becomes

$$\begin{aligned} K &= \left[\begin{array}{ccc} a \left(\xi - (\eta + S) S_\xi \right) & -a(\eta + S) & A - a(\eta + S) S_\zeta \\ a \left(\eta + S + \xi S_\xi \right) & a\xi & B + a\xi S_\zeta \\ 0 & 0 & 1 \end{array} \right] \\ &= \left[\begin{array}{ccc} x_\xi & x_\eta & A + x_\eta S_\zeta \\ y_\xi & y_\eta & B + y_\eta S_\zeta \\ 0 & 0 & 1 \end{array} \right], \end{aligned}$$

where

$$A = a_\zeta \frac{x - x_0}{a} + x_{0_\zeta}, \quad B = a_\zeta \frac{y - y_0}{a} + y_{0_\zeta}.$$

Now,

$$J = x_\xi y_\eta - x_\eta y_\xi = \xi^2 + (\eta + S)^2$$

and

$$J K^{-1} = \left[\begin{array}{ccc} y_\eta & -x_\eta & x_\eta B - y_\eta A \\ -y_\xi & x_\xi & y_\xi A - x_\xi B - J S_\zeta \\ 0 & 0 & J \end{array} \right].$$

Then under a modification δS

$$\begin{aligned} \delta x_\xi &= -a \left(\delta S S_\xi + (\eta + S) \delta S_\xi \right) \\ \delta x_\eta &= -a \delta S \\ \delta y_\xi &= a \left(\delta S + \xi \delta S_\xi \right) \\ \delta y_\eta &= 0. \end{aligned}$$

Thus
$$\delta J = 2a^2 (\eta + \mathcal{S}) \delta \mathcal{S}$$

and

$$\delta \left(J K^{-1} \right) = \begin{bmatrix} 0 & a\delta\mathcal{S} & -a\mathcal{B}\delta\mathcal{S} \\ -\delta y_\xi & \delta x_\xi & \mathcal{D} \\ 0 & 0 & \delta J \end{bmatrix}.$$

where

$$\mathcal{D} = \delta y_\xi \mathcal{A} - \delta x_\xi \mathcal{B} - a_\zeta \frac{J}{a}\delta\mathcal{S} - \delta J \mathcal{S}_\zeta - J\delta\mathcal{S}_z.$$

Inserting these formulas in equation (81) we find that the volume integral in δI is

$$\iiint \frac{\partial \psi^T}{\partial \xi} \delta \mathcal{S} f_2 \, d\xi \, d\eta \, d\zeta$$

$$- \iiint \frac{\partial \psi^T}{\partial \eta} \{-\delta y_\xi f_1 + \delta x_\xi f_2 + \mathcal{D} f_3\} \, d\xi \, d\eta \, d\zeta$$

$$+ \iiint \frac{\partial \psi^T}{\partial \zeta} \delta J f_3 \, d\xi \, d\eta \, d\zeta,$$

where $\mathcal{S}$ and $\delta\mathcal{S}$ are independent of η. Therefore, integrating over η, the variation in the cost function can be reduced to a surface integral of the form

$$\delta I = \iint_{B_w} \left(P(\xi,\zeta)\delta\mathcal{S} - Q(\xi,\zeta)\delta\mathcal{S}_\xi - R(\xi,\zeta)\delta\mathcal{S}_\zeta \right) d\xi \, d\zeta$$

Here

$$\begin{aligned}
P &= a \left(\psi_2 + \mathcal{S}_\xi \psi_3 + \mathcal{C}\psi_4 \right) p \\
&\quad - \int \frac{\partial \psi^T}{\partial \xi} \{\xi f_1 + (\eta + \mathcal{S}) f_2 + (\xi\mathcal{A} + (\eta + \mathcal{S})\mathcal{B}) f_3\} \, d\eta \\
&\quad - \int \frac{\partial \psi^T}{\partial \eta} \left(f_1 + \mathcal{S}_\xi f_2 + \mathcal{C} f_3 \right) d\eta \\
&\quad - \int \frac{\partial \psi^T}{\partial \zeta} J \, d\eta
\end{aligned}$$

$$\begin{aligned}
Q &= a(\xi\psi_2 + (\eta + \mathcal{S})\psi_3)p \\
&\quad + \int \frac{\partial \psi^T}{\partial \eta} \{\xi f_1 + (\eta + \mathcal{S}) f_2 + (\xi\mathcal{A} + (\eta + \mathcal{S})\mathcal{B}) f_3\} \, d\eta
\end{aligned}$$

$$\begin{aligned}
R &= J\psi_4 p \\
&\quad + \int \frac{\partial f_3}{\partial \eta} J\psi_4 d\eta,
\end{aligned}$$

where

$$\mathcal{C} = 2a(\eta + \mathcal{S})\mathcal{S}_\zeta - \mathcal{A} - \mathcal{B}\mathcal{S}_\xi + \frac{J}{a}.$$

Also the shape change will be confined to a boundary region of the $\xi - \zeta$ plane, so we can integrate by parts to obtain

$$\delta I = \iint_{B_w} \left(P + \frac{\partial Q}{\partial \xi} + \frac{\partial R}{\partial \zeta} \right) \delta \mathcal{S} \, d\xi \, d\zeta.$$

Thus to reduce I we can choose

$$\delta \mathcal{S} = -\lambda \left(P + \frac{\partial Q}{\partial \xi} + \frac{\partial R}{\partial \zeta} \right),$$

where λ is sufficiently small and non-negative.

In order to impose a thickness constraint we can define a baseline surface $\mathcal{S}_0(\xi,\zeta)$ below which $\mathcal{S}(\xi,\zeta)$ is not allowed to fall. Now if we take $\lambda = \lambda(\xi,\zeta)$ as a non-negative function such that

$$\mathcal{S}(\xi,\zeta) + \delta\mathcal{S}(\xi,\zeta) \geq \mathcal{S}_0(\xi,\zeta).$$

Then the constraint is satisfied, while

$$\delta I = - \iint_{B_w} \lambda \left(P + \frac{\partial Q}{\partial \xi} + \frac{\partial R}{\partial \zeta} \right)^2 d\xi \, d\zeta \leq 0.$$

9 IMPLEMENTATION OF THE THREE DIMENSIONAL METHOD FOR WING DESIGN

Since three dimensional calculations are much more expensive than two dimensional calculations, it is extremely important for the practical implementation of the method to use fast solution algorithms for the flow and the adjoint equations. In this case the author's FLO87 computer program has been used as the basis of the design method. FLO87 solves the three dimensional Euler equations with a cell-centered finite volume scheme, and uses residual averaging and multigrid acceleration to obtain very rapid steady state solutions, usually in 25 to 50 multigrid cycles [8, 9]. Upwind biasing is used to produce nonoscillatory solutions, and assure the clean capture of shock waves. This is introduced through the addition of carefully controlled numerical diffusion terms, with a magnitude of order Δx^3 in smooth parts of the flow. The program corresponds closely to FLO82, which was used to implement the design method for the two dimensional Euler equations. The adjoint equations are treated in the same way as the flow equations. The fluxes are first estimated by central differences, and then modified by downwind biasing through numerical diffusive terms which are supplied by the same subroutines that were used for the flow equations.

The method has been tested for the optimization of a swept wing. The planform was fixed while the wing sections were free to be changed arbitrarily by the design method. The wing has a unit-semi-span, with 36 degrees leading edge sweep. It has a compound trapezoidal planform, with straight taper from a root chord of 0.38 to a chord of 0.26 at the 30 percent span station, and straight taper from there to a chord of 0.12 at the tip, with an aspect ratio of 8.7. The initial wing sections were based on the Korn airfoil, which was designed for shock free flow at Mach 0.75 with a lift coefficient of 0.63, and has a thickness to chord ratio of 11.5 percent [1]. The thickness to chord ratio was increased by a factor of 1.2 at the root and decreased by a ratio of 0.8 at the tip, with a linear variation across the span. The inboard sections were rotated upwards to give 3.5 degrees twist across the span.

The two dimensional pressure distribution of the Korn airfoil at its design point was introduced as a target pressure distribution uniformly across the span. This target is

presumably not realizable, but serves to favor the establishment of relatively benign pressure distribution. The total inviscid drag coefficient, due to the combination of vortex and shock wave drag, was also included in the cost function. Calculations were performed with the lift coefficient forced to approach a fixed value by adjusting the angle of attack every fifth iteration of the flow solution. It was found that the computational costs can be reduced by using only 15 multigrid cycles in each flow solution, and in each adjoint solution. Although this is not enough for full convergence, it proves sufficient to provide a shape modification which leads to an improvement. Figures 15,16, and 17 show the result of a calculation at Mach number of 0.82, with the lift coefficient forced to approach a value of 0.5. This calculation was performed on a mesh with 192 intervals in the ξ direction wrapping around the wing, 32 intervals in the normal η direction and 48 intervals in the spanwise ζ direction, giving a total of 294912 cells. The wing was specified by 33 sections, each with 128 points, giving a total of 4224 design variables. The plots show the initial wing geometry and pressure distribution, and the modified geometry and pressure distribution after 8 design cycles. The total inviscid drag was reduced from 0.0185 to 0.0118. The initial design exhibits a very strong shock wave in the inboard region. It can be seen that this is completely eliminated, leaving a very weak shock wave in the outboard region. The drag reduction is mainly accomplished in the first four design cycles but the pressure distribution continues to be adjusted to become more like the Korn pressure distribution.

To verify the solution, the final geometry, after 8 design cycles, was analyzed with another method using the computer program FLO67. This program uses a cell-vertex formulation, and has recently been modified to incorporate a local extremum diminishing algorithm with a very low level of numerical diffusion [12]. When run to full convergence it was found that the redesigned wing has a drag coefficient of 0.0107 at Mach 0.82 at a lift coefficient of 0.5, with a corresponding lift to drag ratio of 47. The result is illustrated in Figure 18. A calculation at Mach 0.500 shows a drag coefficient of 0.0100 for a lift coefficient of 0.5. Since in this case the flow is entirely subsonic, this provides an estimate of the vortex drag for this planform and lift distribution. Thus the design method has reduced the shock wave drag coefficient to about 0.0007. For a representative transport aircraft the parasite drag coefficient of the wing due to skin friction is about 0.0050. Also the fuselage drag coefficient is about 0.0050, the nacelle drag coefficient is about 0.0015, the empennage drag coefficient is about 0.0015, and excrescence drag coefficient is about 0.0006. This would give a total drag coefficient $C_D = 0.0243$ for a lift coefficient of 0.5, corresponding to a lift to drag ratio $L/D = 20.5$. This would be a substantial improvement over the values obtained by currently flying transport aircraft.

As a further test the redesign was also performed at a higher Mach number of 0.85. The initial geometry

and pressure distributions, and the result of the redesign after 10 design cycles are displayed in Figures 19, 20 and 21. In this case the total inviscid drag was reduced from 0.0261 to 0.0132. Again this result has been checked with FLO67, and when the flow calculation is fully converged, it is found that the total inviscid drag coefficient is 0.0118 at a lift coefficient of 0.5, indicating a shock wave drag coefficient of 0.0018. Allowing for the other sources of drag for the complete aircraft, it is likely that the best operating point for maximum lift to drag ratio would be at a somewhat higher lift coefficient.

10 CONCLUSION

In the period since this approach to optimal shape design was first proposed by the author [10], the method has been verified by numerical implementation for both potential flow and flows modeled by the Euler equations. It has been demonstrated that it can be successfully used with a finite volume formulation to perform calculations with arbitrary numerically generated grids [16]. The first results which have been obtained for swept wings with the three dimensional Euler equations suggest that the method has now matured to the point where it can be a very useful tool for the design of new airplanes. Even in the case of three dimensional flows, the computational requirements are so moderate that the calculations can be performed with workstations such as the IBM RISC 6000 series. A design cycle on a 192x32x48 mesh takes about $1\frac{1}{2}$ hours on an IBM model 530 workstation, allowing overnight completion of a design calculation for a swept wing.

11 ACKNOWLEDGMENTS

References

[1] F. Bauer, P. Garabedian, D. Korn, and A. Jameson. *Supercritical Wing Sections II*. Springer Verlag, New York, 1975.

[2] O. Baysal and M. E. Eleshaky. Aerodynamic design optimization using sensitivity anaysis and computational fluid dynamics. *AIAA paper 91-0471*, 29th

18

Aerospace Sciences Meeting, Reno, Nevada, January 1991.

[3] M.O. Bristeau, O. Pironneau, R. Glowinski, J. Periaux, P. Perrier, and G. Poirier. On the numerical solution of nonlinear problems in fluid dynamics by least squares and finite element methods (II). application to transonic flow simulations. In J. St. Doltsinis, editor, *Proceedings of the 3rd International Conference on Finite Element Methods in Nonlinear Mechanics, FENOMECH 84, Stuttgart, 1984*, pages 363–394, North Holland, 1985.

[4] P.E. Gill, W. Murray, and M.H. Wright. *Practical Optimization*. Academic Press, 1981.

[5] R. M. Hicks and P. A. Henne. Wing design by numerical optimization. *Journal of Aircraft*, 15:407–412, 1978.

[6] A. Jameson. Iterative solution of transonic flows over airfoils and wings, including flows at Mach 1. *Communications on Pure and Applied Mathematics*, 27:283–309, 1974.

[7] A. Jameson. Acceleration of transonic potential flow calculations on arbitrary meshes by the multiple grid method. *AIAA paper 79-1458*, Fourth AIAA Computational Fluid Dynamics Conference, Williamsburg, Virginia, July 1979.

[8] A. Jameson. Solution of the Euler equations by a multigrid method. *Applied Mathematics and Computations*, 13:327–356, 1983.

[9] A. Jameson. Multigrid algorithms for compressible flow calculations. In W. Hackbusch and U. Trottenberg, editors, *Lecture Notes in Mathematics, Vol. 1228*, pages 166–201. Proceedings of the 2nd European Conference on Multigrid Methods, Cologne, 1985, Springer-Verlag, 1986.

[10] A. Jameson. Aerodynamic design via control theory. *Journal of Scientific Computing*, 3:233–260, 1988.

[11] A. Jameson. Automatic design of transonic airfoils to reduce the shock induced pressure drag. In *Proceedings of the 31st Israel Annual Conference on Aviation and Aeronautics, Tel Aviv*, pages 5–17, February 1990.

[12] A. Jameson. Artificial diffusion, upwind biasing, limiters and their effect on accuracy and multigrid convergence in transonic and hypersonic flows. *AIAA paper 93-3359*, AIAA 11th Computational Fluid Dynamics Conference, Orlando, Florida, July 1993.

[13] M.J. Lighthill. A new method of two-dimensional aerodynamic design. *R & M 1111*, Aeronautical Research Council, 1945.

[14] J.L. Lions. *Optimal Control of Systems Governed by Partial Differential Equations*. Springer-Verlag, New York, 1971. Translated by S.K. Mitter.

[15] O. Pironneau. *Optimal Shape Design for Elliptic Systems*. Springer-Verlag, New York, 1984.

[16] J. Reuther and A. Jameson. Control theory based airfoil design for potential flow and a finite volume discretization. *AIAA paper 91-499*, 32th Aerospace Sciences Meeting and Exibit, Reno, Nevada, January 1994.

[17] J. Reuther, C.P. van Dam, and R. Hicks. Subsonic and transonic low-Reynolds-number airfoils with reduced pitching moments. *Journal of Aircraft*, 29:297–298, 1992.

[18] G. R. Shubin. Obtaining cheap optimization gradients from computaional aerodynamics codes. *Internal paper AMS-TR-164*, Boeing Computer Services, June 1991.

[19] G. R. Shubin and P. D. Frank. A comparison of the implicit gradient approach and the variational approach to aerodynamic design optimization. *internal paper AMS-TR-164*, Boeing Computer Services, April 1991.

[20] S. Ta'asan, G. Kuruvila, and M. D. Salas. Aerodynamic design and optimization in one shot. *AIAA paper 91-005*, 30th Aerospace Sciences Meeting and Exibit, Reno, Nevada, January 1992.
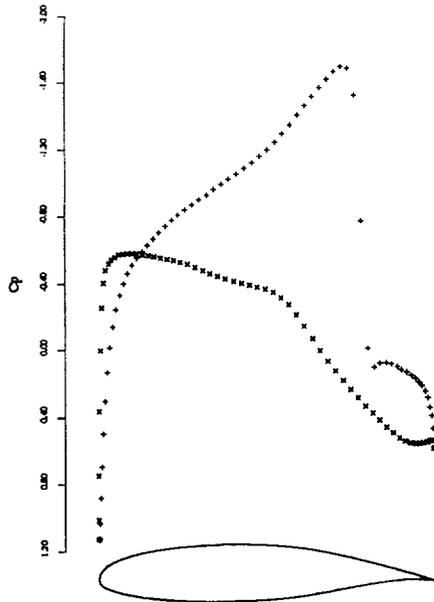
3a: C_p after Zero Design Cycles.
Design Mach 0.72, $C_l = 0.5982, C_d = 0.0191$.
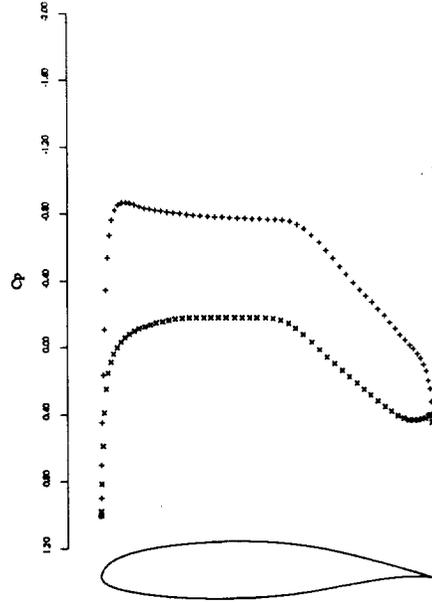
3b: C_p after Zero Design Cycles.
Design Mach 0.2, $C_l = 0.5998, C_d = -0.0001$.
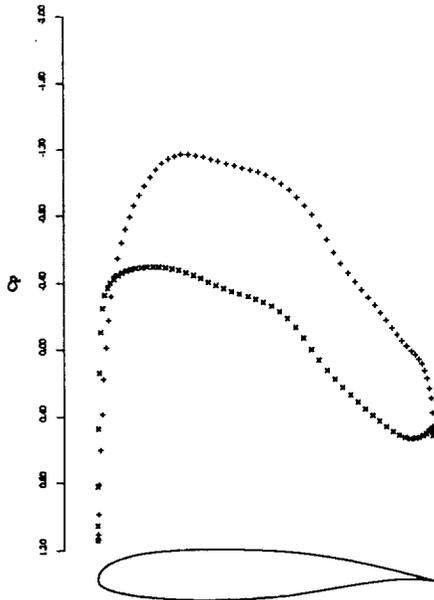
3c: C_p after Eight Design Cycles.
Design Mach 0.72, $C_l = 0.5999, C_d = 0.0001$.
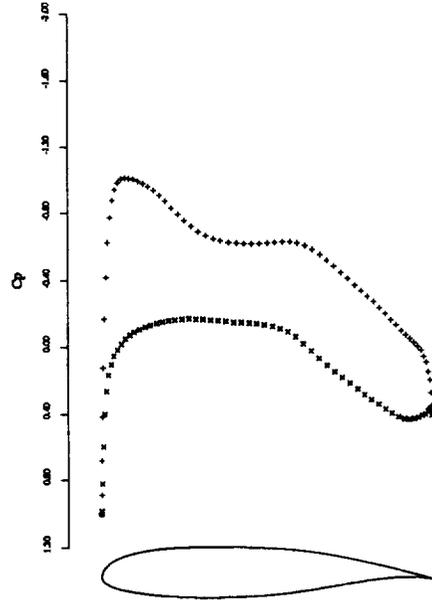
3d: C_p after Eight Design Cycles.
Design Mach 0.2, $C_l = 0.5998, C_d = -0.0001$.

Figure 3: Optimization of an Airfoil at Two Design Points.
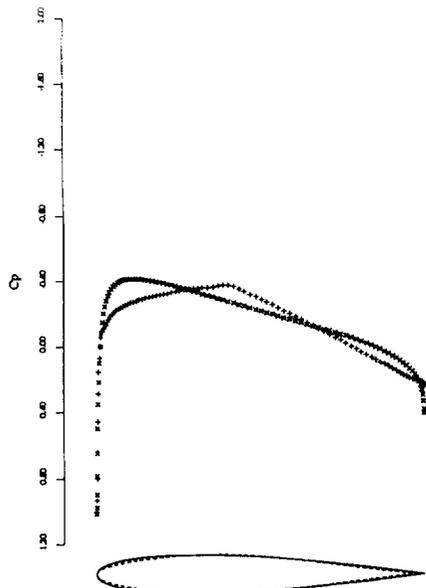
4a: Initial Condition
$C_l = 0.0000, C_d = 0.0001$
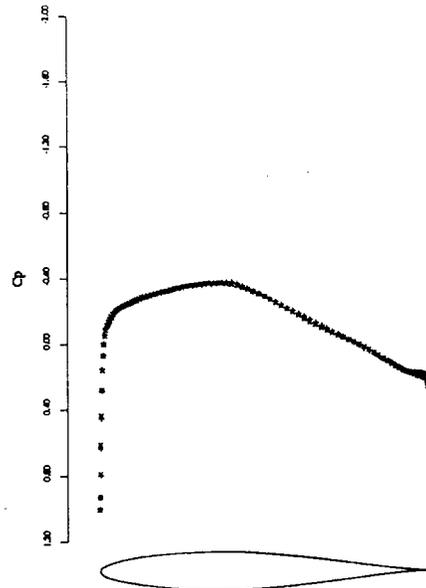
4b: 7 Design Iterations
$C_l = 0.0000, C_d = 0.0000$

Figure 4: Subsonic Non-Lifting Design Case, $M = 0.2, \alpha = 0°$.
—, × Initial Airfoil: NACA 0012.
- - -, + Target C_p: NACA 64012, $M = 0.2$.
Inverse Design
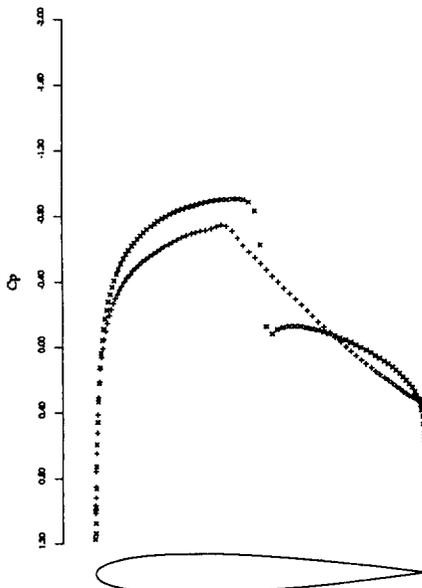
5a: Initial Condition
$C_l = 0.0000, C_d = 0.0063$
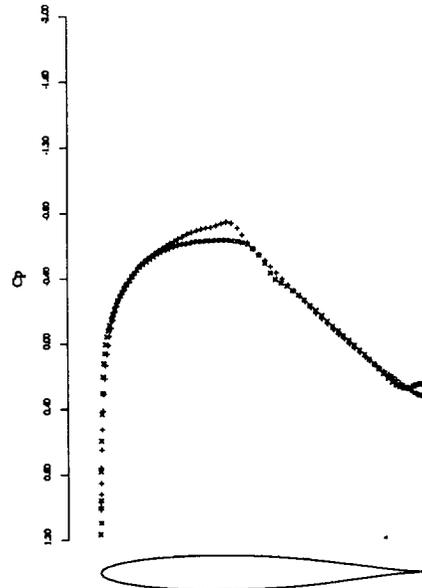
5b: 7 Design Iterations
$C_l = 0.0000, C_d = 0.0003$

Figure 5: Transonic Non-Lifting Design Case, $M = 0.8$ $\alpha = 0°$.
—, × Initial Airfoil: NACA 0012.
- - -, + Target C_p: NACA 64021, $M = 0.2$.
Inverse Design

21
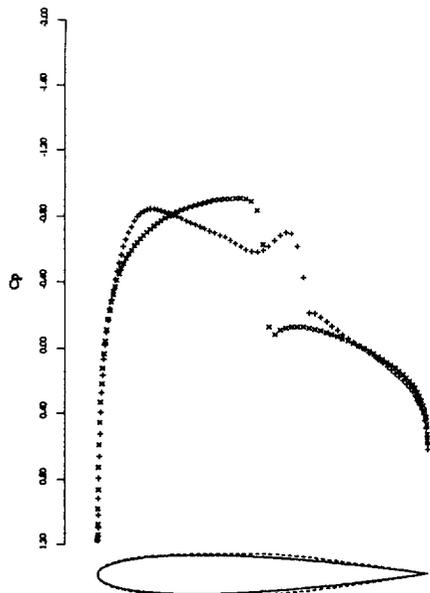
6a: Initial Condition
$C_l = 0.0000, C_d = 0.0063$
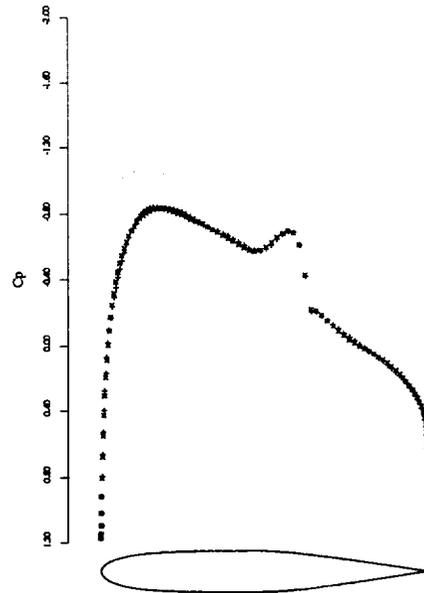
6b: 8 Design Iterations
$C_l = 0.0000, C_d = 0.0015$

Figure 6: Transonic Non-Lifting Design Case, $M = 0.8, \alpha = 0°$.
—, $\times$ Initial Airfoil: NACA 0012.
- - -, + Target C_p: NACA 64X, $M = 0.8$.
Inverse Design
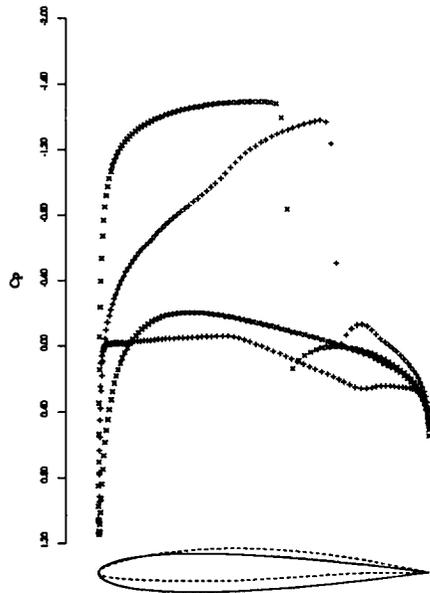
7a: Initial Condition
$C_l = 0.7315, C_d = 0.0252, \alpha = 2.664°$
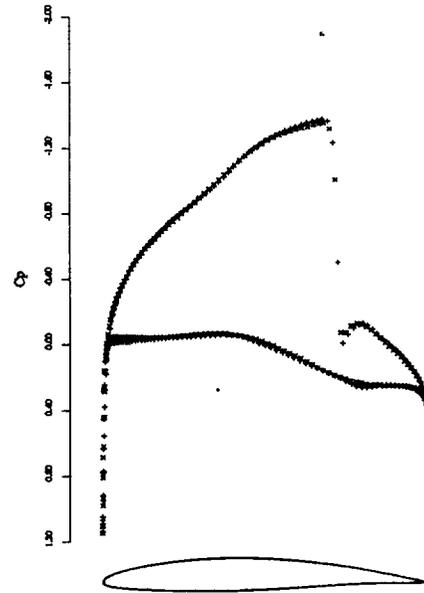
7b: 20 Design Iterations
$C_l = 0.7334, C_d = 0.0086, \alpha = 0.032°$

Figure 7: Transonic Lifting Design Case, $M = 0.735$ Fixed Lift.
—, $\times$ Initial Airfoil: NACA 0012.
- - -, + Target C_p: NACA 64A410, $M = 0.735, C_l = 0.73$.
Inverse Design
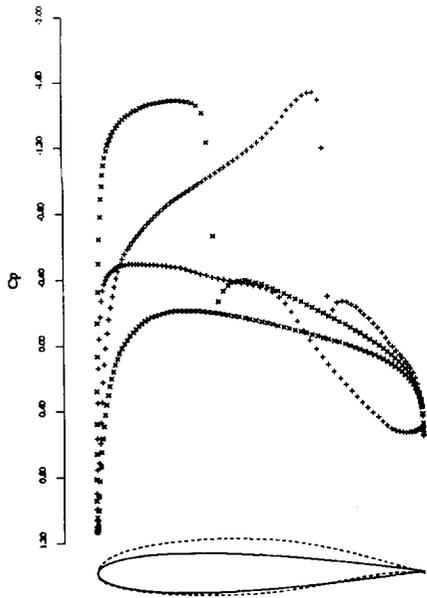
8a: Initial Condition
$C_l = 0.5492, C_d = 0.0047, \alpha = 2.709°$
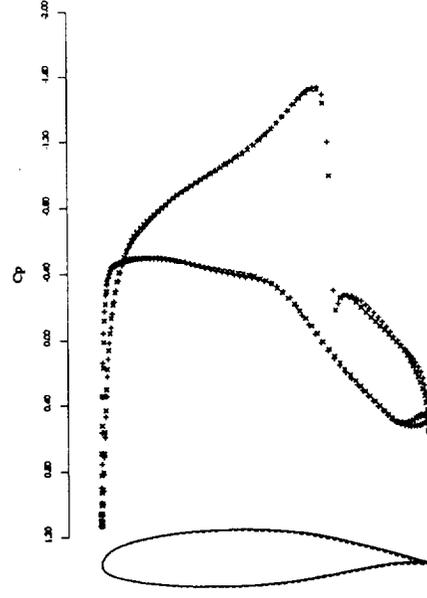
8b: 30 Design Iterations
$C_l = 0.5496, C_d = 0.0045, \alpha = -1.508°$

Figure 8: Transonic Lifting Design Case, $M = 0.70$, Fixed Lift.
—, × Initial Airfoil: NACA 0012.
- - -, + Target C_p: GAW72, $M = 0.70$.
Inverse Design
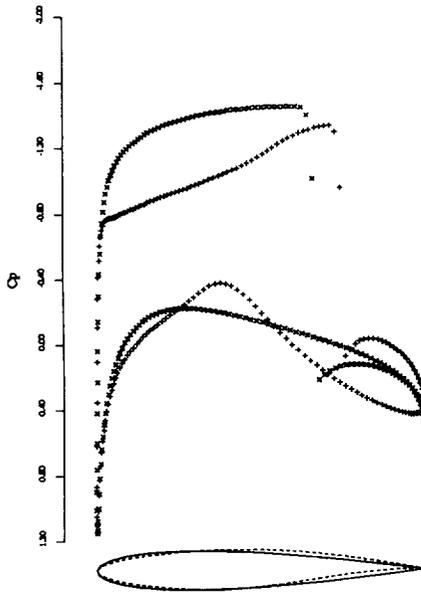
9a: Initial Condition
$C_l = 0.7946, C_d = 0.0358, \alpha = 2.364°$
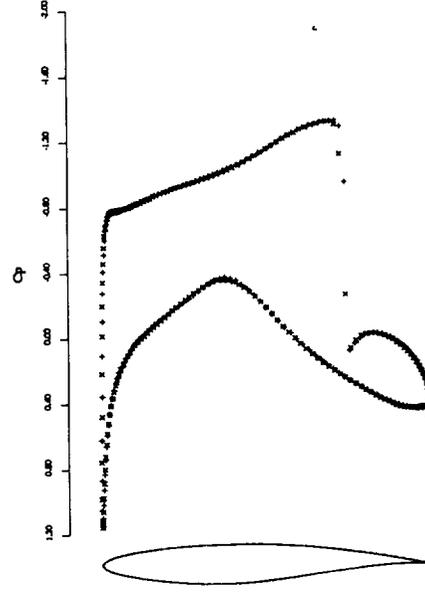
9b: 27 Design Iterations
$C_l = 0.7971, C_d = 0.0108, \alpha = 1.053°$

Figure 9: Transonic Lifting Design Case, $M = 0.75$ Fixed Lift.
—, × Initial Airfoil: NACA 0012.
- - -, + Target C_p: RAE, $M = 0.75$.
Inverse Design

23
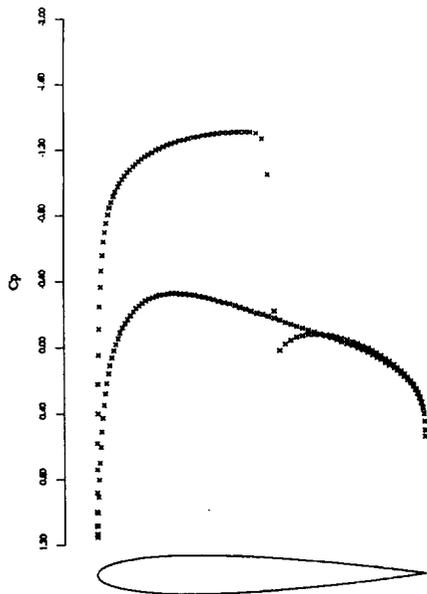
10a: Initial Condition
$C_l = 0.5037, C_d = 0.0127, \alpha = 1.856°$
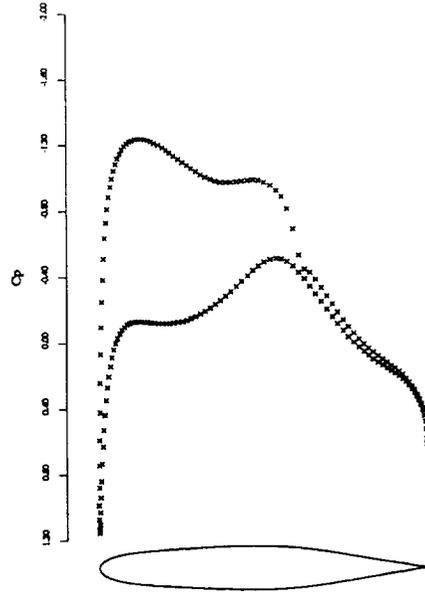
10b: 2 Design Iterations
$C_l = 0.5042, C_d = 0.0016, \alpha = 1.990°$

Figure 10: Transonic Lifting Design Case, $M = 0.75$, Fixed Lift.
—, × Initial Airfoil: NACA 0012.
Symetric Drag Minimization.
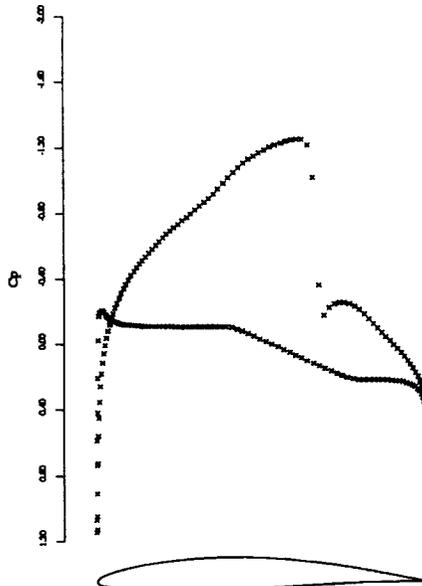
11a: Initial Condition
$C_l = 0.5964, C_d = 0.0042, \alpha = -0.464°$
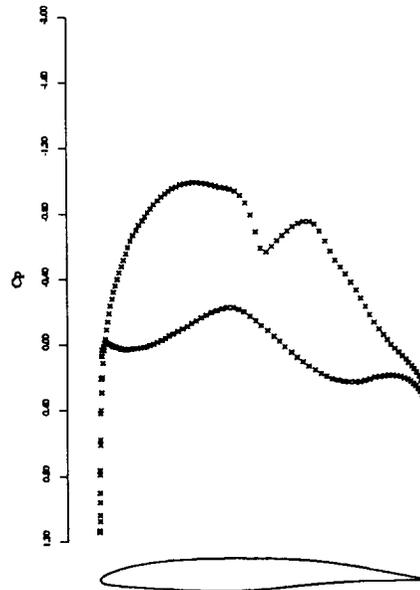
11b: 2 Design Iterations
$C_l = 0.5966, C_d = 0.0004, \alpha = 0.175°$

Figure 11: Transonic Lifting Design Case, $M = 0.735$ Fixed Lift.
—, × Initial Airfoil: NACA 64A410.
Camber Only Drag Minimization.

24
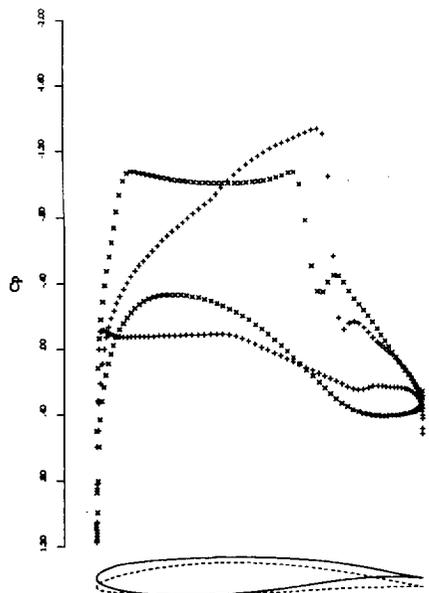
12a: Initial Condition
$C_l = 0.7019, C_d = 0.0015, \alpha = 0.266°$
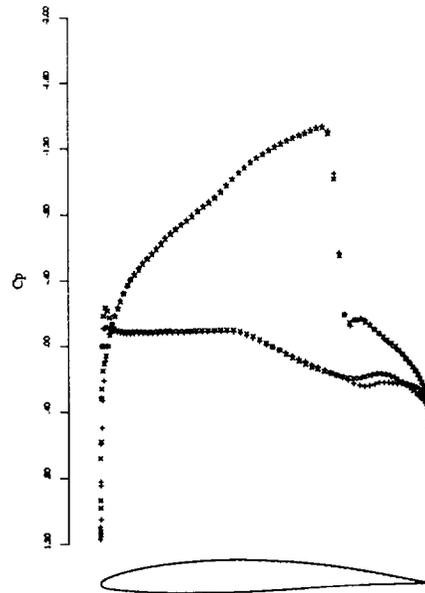
12b: 40 Design Iterations
$C_l = 0.6612, C_d = 0.0136, \alpha = -0.037°$

Figure 12: Lifting Design Case, $M = 0.75$, Fixed Lift Mode.
—, × Initial Airfoil: Korn.
- - -, + Target C_p: NACA 64012, $M = 0.75$.
Inverse Design
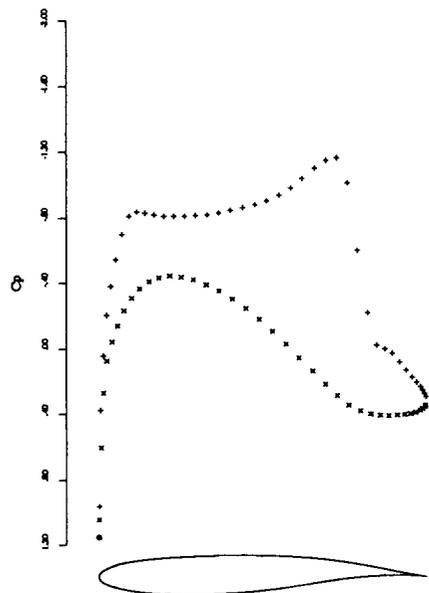
13a: Initial Condition
$C_l = 0.6432, C_d = 0.0155, \alpha = -0.229°$
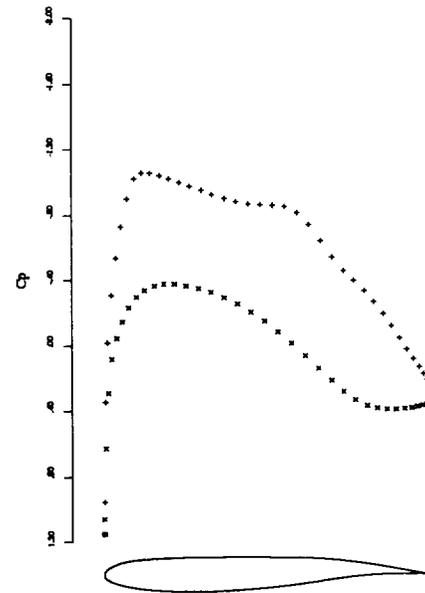
13b: 20 Design Iterations
$C_l = 0.6297, C_d = 0.0077, \alpha = 0.033°$

Figure 13: Lifting Design Case, $M = 0.78$ Fixed Lift Mode
Initial Airfoil: Korn.
Target C_p: Korn, $M = 0.75$.
Inverse Design

25
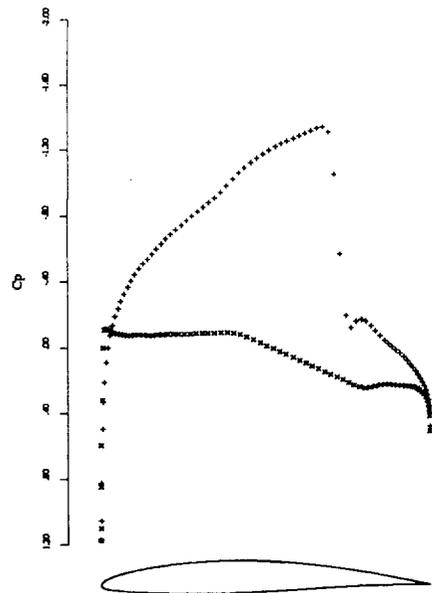
14a: Initial Condition
$C_l = 0.6778, C_d = 0.0144, \alpha = -0.096°$
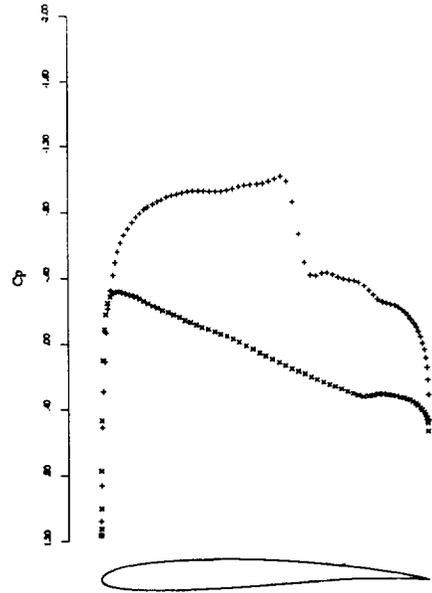
14b: 25 Design Iterations
$C_l = 0.6855, C_d = 0.0010, \alpha = -0.722°$

Figure 14: Lifting Design Case, $M = 0.75$, Fixed Lift Mode.
Initial Airfoil: NACA 64A410.
Drag Reduction
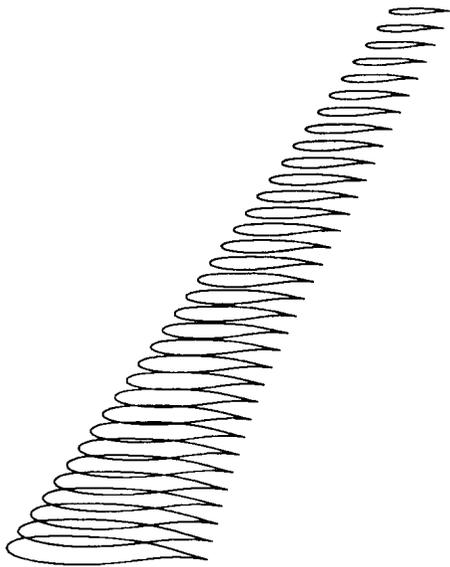
15a: Initial Wing
$C_l = 0.5001, C_d = 0.0185, \alpha = -0.958°$
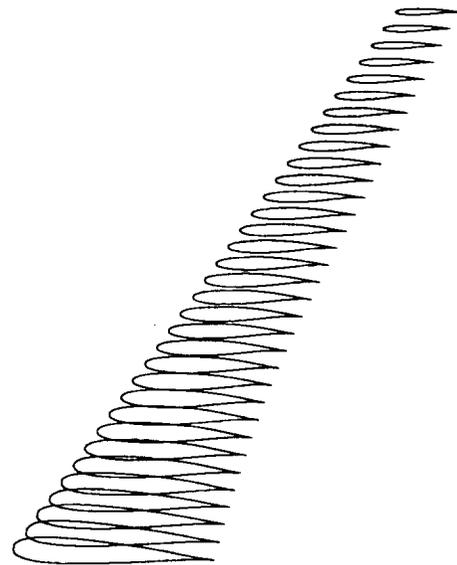
15b: 8 Design Iterations
$C_l = 0.4929, C_d = 0.0118, \alpha = 0.172°$

Figure 15: Lifting Design Case, $M = 0.82$, Fixed Lift Mode.
Drag Reduction
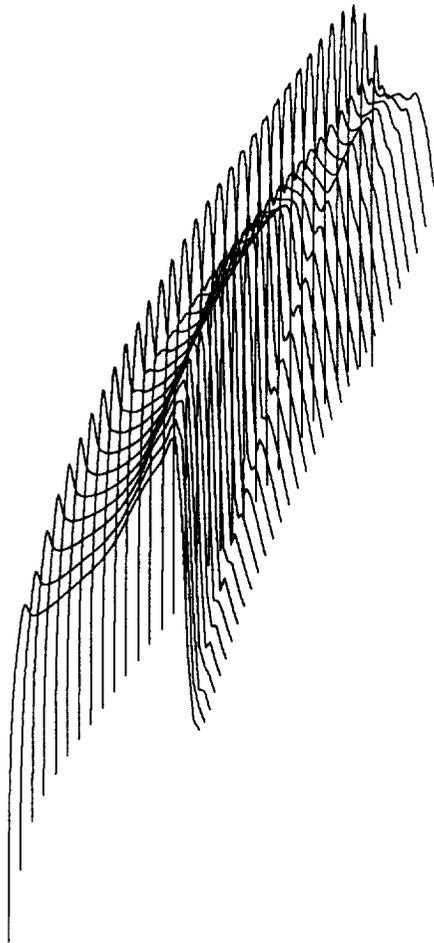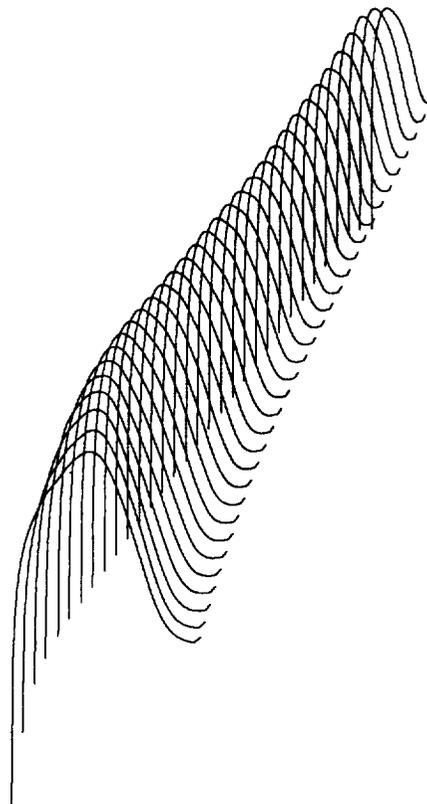
UPPER SURFACE PRESSURE   LOWER SURFACE PRESSURE

Figure 16: Lifting Design Case, $M = 0.82$, Fixed Lift Mode.
Initial Wing: Modfied Korn.
$C_L = 0.5001, C_D = 0.0185, \alpha = -0.958°$
Drag Reduction
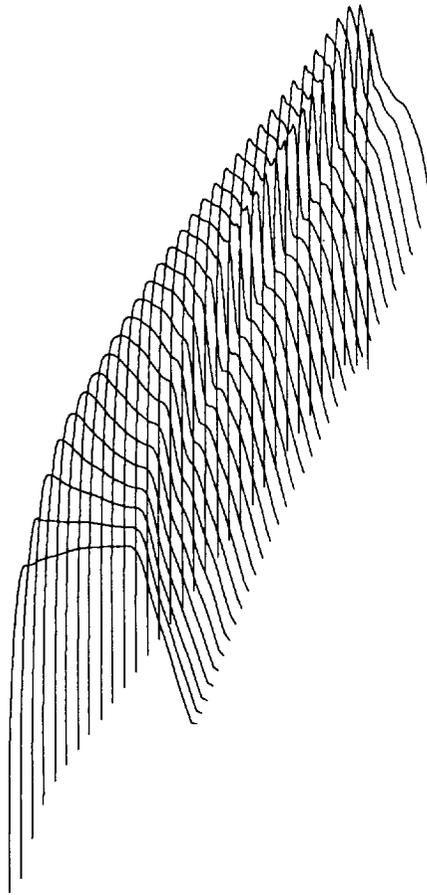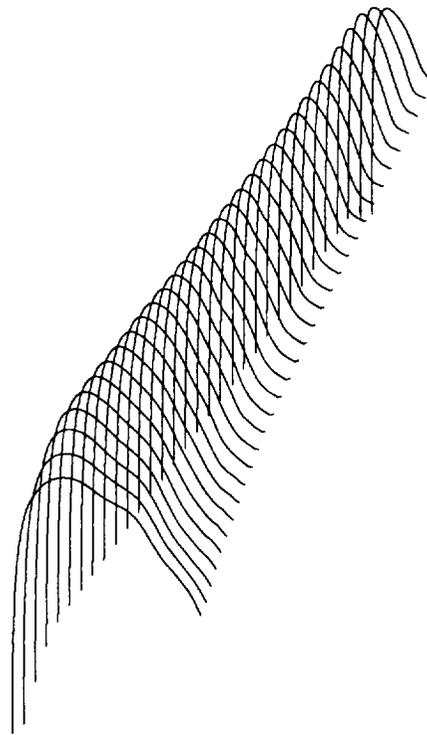
UPPER SURFACE PRESSURE   LOWER SURFACE PRESSURE

Figure 17: Lifting Design Case, $M = 0.82$, Fixed Lift Mode.
Design after 8 cycles
$C_L = 0.4929, C_D = 0.0118, \alpha = 0.172°$
Drag Reduction
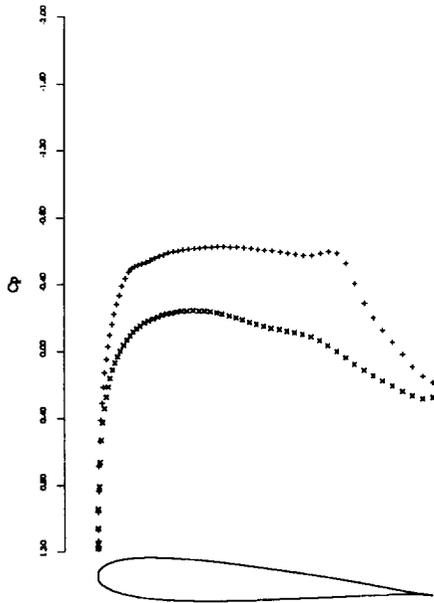
18a: span station $z = 0.00$
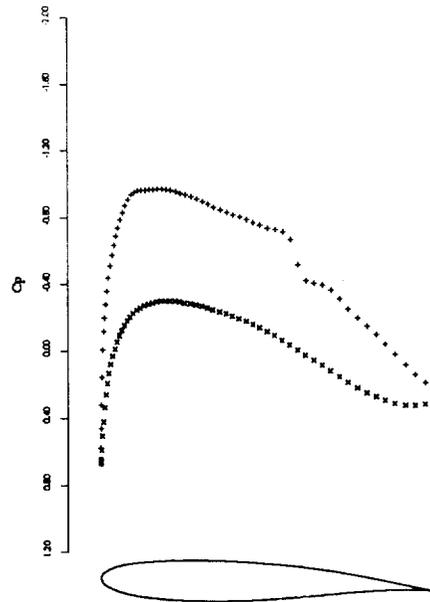
18b: span station $z = 0.25$
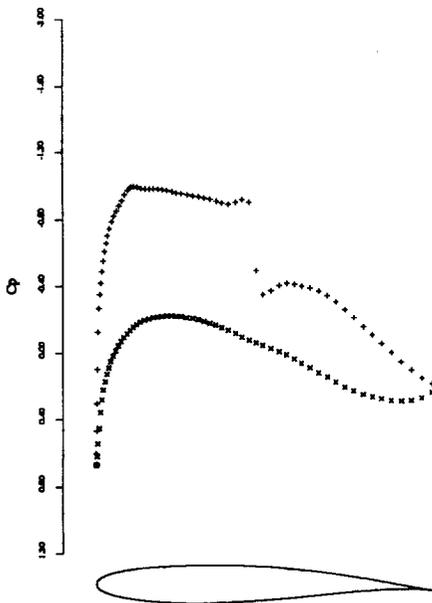
18c: span station $z = 0.50$
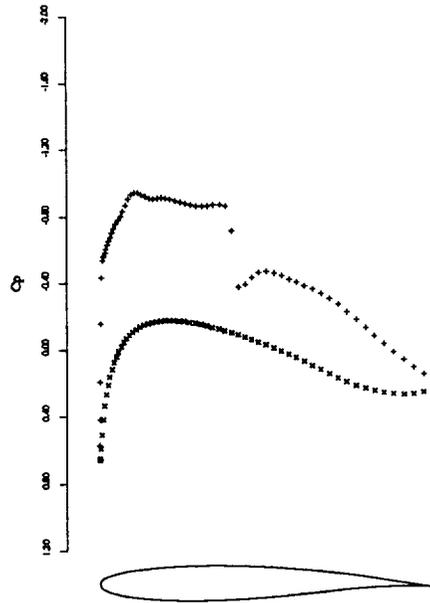
18d: span station $z = 0.75$

Figure 18: FLO67 check on redesigned wing.
$M = 0.82, C_L = 0.4975, C_D = 0.0107, \alpha = 0.200°$
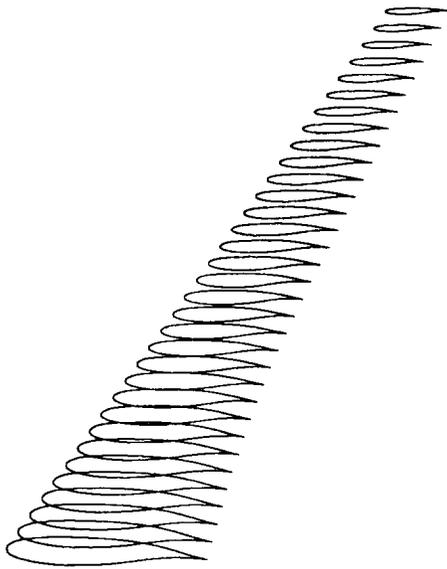
19a: Initial Wing
$C_l = 0.5033, C_d = 0.0261, \alpha = -1.236°$
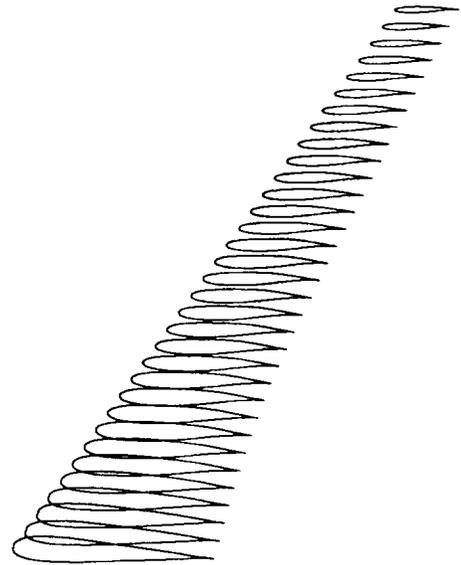
19b: 10 Design Iterations
$C_l = 0.4956, C_d = 0.0132, \alpha = -0.028°$

Figure 19: Lifting Design Case, $M = 0.85$, Fixed Lift Mode.
Drag Reduction
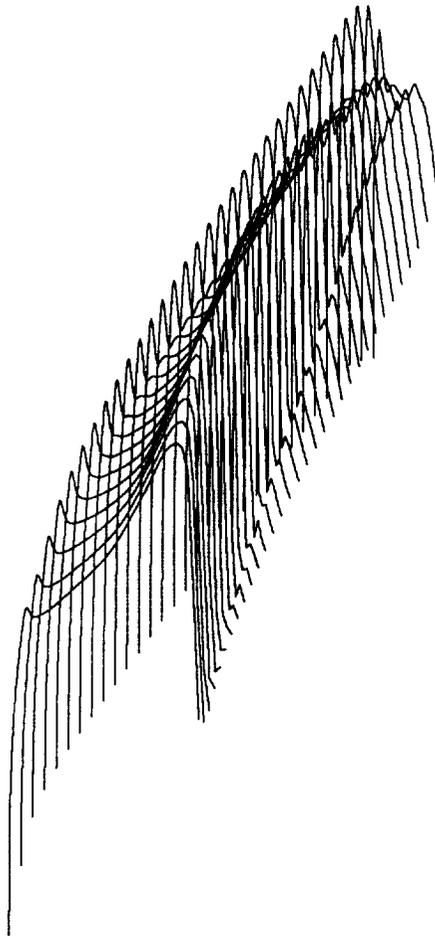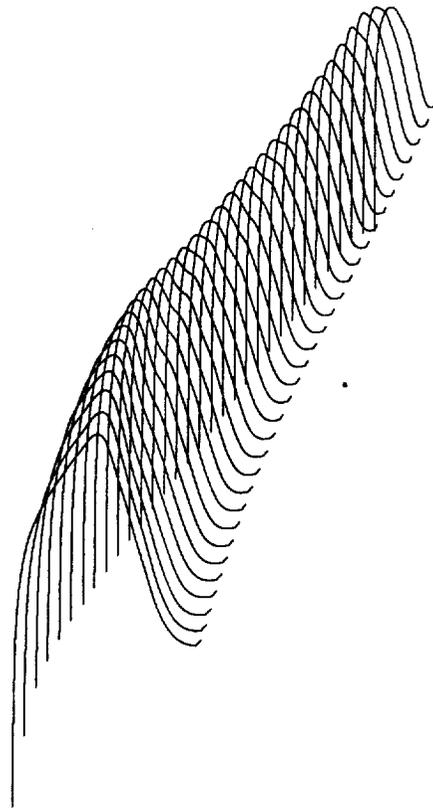
UPPER SURFACE PRESSURE   LOWER SURFACE PRESSURE

Figure 20: Lifting Design Case, $M = 0.85$, Fixed Lift Mode.
Initial Airfoil: Modified Korn.
$C_L = 0.5033, C_D = 0.0261, \alpha = -1.236°$
Drag Reduction
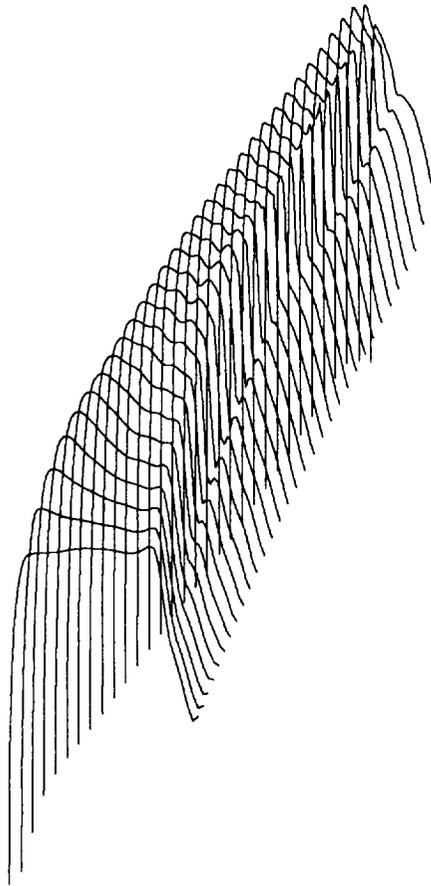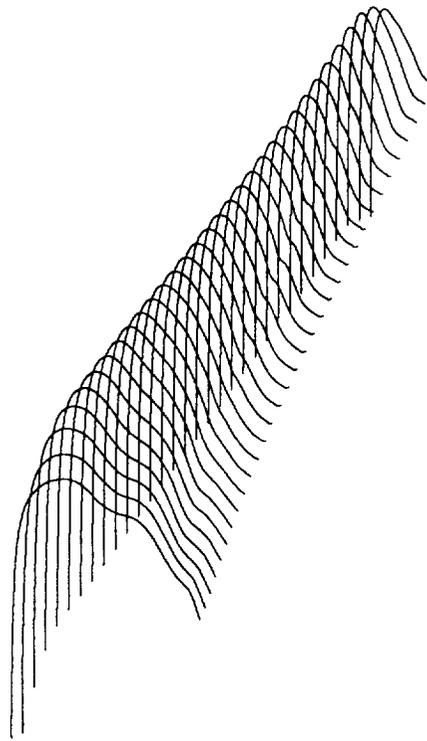
UPPER SURFACE PRESSURE   LOWER SURFACE PRESSURE

Figure 21: Lifting Design Case, $M = 0.85$, Fixed Lift Mode.
Design after 10 cycles
$C_L = 0.4956, C_D = 0.0132, \alpha = -0.028°$
Drag Reduction